Immunity

CellPress

Article

In Situ Maturation and Tissue Adaptation of Type 2 Innate Lymphoid Cell Progenitors

Patrice Zeis,[1,3,4,13] Mi Lian,[2,4,5,13] Xiying Fan,[6,13] Josip S. Herman,[1,3,4] Daniela C. Hernandez,[10,11] Rebecca Gentek,[7] Shlomo Elias,[6] Cornelia Symowski,[8] Konrad Knöpper,[2] Nina Peltokangas,[1,4] Christin Friedrich,[2,5] Remi Doucet-Ladeveze,[2] Agnieszka M. Kabat,[1] Richard M. Locksley,[12] David Voehringer,[8] Marc Bajenoff,[7] Alexander Y. Rudensky,[6] Chiara Romagnani,[10,11] Dominic Grün,[1,9,14,15,16,*] and Georg Gasteiger[2,5,14,15,*]

[1]Max Planck Institute of Immunobiology and Epigenetics, Freiburg, Germany
[2]Würzburg Institute of Systems Immunology, Max Planck Research Group at the Julius-Maximilians-Universität Würzburg, Würzburg, Germany
[3]International Max Planck Research School for Molecular and Cellular Biology (IMPRS-MCB), Freiburg, Germany
[4]Faculty of Biology, University of Freiburg, Freiburg, Germany
[5]Institute of Medical Microbiology and Hygiene, University Medical Center Freiburg, Freiburg, Germany
[6]Howard Hughes Medical Institute, Immunology Program, and Ludwig Center, Memorial Sloan Kettering Cancer Center, New York, NY, USA
[7]Aix Marseille Université, CNRS, INSERM, CIML, Marseille, France
[8]Department of Infection Biology, University Hospital Erlangen and Friedrich-Alexander University Erlangen-Nuremberg (FAU), Erlangen, Germany
[9]CIBSS-Centre for Integrative Biological Signaling Studies, University of Freiburg, Freiburg, Germany
[10]German Rheumatism Research Center (DRFZ), Leibniz Association, Berlin, Germany
[11]Medical Department I, Charité-Universitätsmedizin Berlin, Berlin, Germany
[12]Howard Hughes Medical Institute and Department of Medicine, University of California, San Francisco, San Francisco, CA, USA
[13]These authors contributed equally
[14]These authors contributed equally
[15]Senior author
[16]Lead Contact
*Correspondence: gruen@ie-freiburg.mpg.de (D.G.), georg.gasteiger@uni-wuerzburg.de (G.G.)
https://doi.org/10.1016/j.immuni.2020.09.002

SUMMARY

Innate lymphoid cells (ILCs) are generated early during ontogeny and persist predominantly as tissue-resident cells. Here, we examined how ILCs are maintained and renewed within tissues. We generated a single cell atlas of lung ILC2s and found that Il18r1$^+$ ILCs comprise circulating and tissue-resident ILC progenitors (ILCP) and effector-cells with heterogeneous expression of the transcription factors Tcf7 and Zbtb16, and CD103. Our analyses revealed a continuous differentiation trajectory from Il18r1$^+$ ST2$^-$ ILCPs to Il18r$^-$ ST2$^+$ ILC2s, which was experimentally validated. Upon helminth infection, recruited and BM-derived cells generated the entire spectrum of ILC2s in parabiotic and shield chimeric mice, consistent with their potential role in the renewal of tissue ILC2s. Our findings identify local ILCPs and reveal ILCP *in situ* differentiation and tissue adaptation as a mechanism of ILC maintenance and phenotypic diversification. Local niches, rather than progenitor origin, or the developmental window during ontogeny, may dominantly imprint ILC phenotypes in adult tissues.

INTRODUCTION

Innate lymphoid cells (ILCs) have been identified in many different tissues where they contribute to immune surveillance, tissue homeostasis and repair, and barrier function. ILCs are found in the bone marrow, in secondary lymphoid organs, and, most prominently, in non-lymphoid tissues including mucosal barriers. The size and subset composition of the local pool of ILCs can dramatically vary between organs and is further shaped in response to environmental challenges. Despite considerable progress in ILC biology, their local differentiation and adaptation to heterogeneous tissue environments remain poorly understood.

ILC progenitors can seed tissues during embryonic development (Bando et al., 2015). In many tissues, ILCs expand and differentiate during the first weeks of life (Saluzzo et al., 2017; Schneider et al., 2019), after which they persist predominantly as tissue-resident effector cells. Originally established in parabiotic mice (Gasteiger et al., 2015; Huang et al., 2018; Moro et al., 2016; Peng et al., 2013), this concept is supported by analyses of human ILCs in transplanted livers and intestines (Cuff et al., 2016; Weiner et al., 2017). Consistently, a fraction of ILC2s labeled in the neonatal window persists in adult tissues (Schneider et al., 2019). Yet, these observations also highlight that ILCs may also be generated during adult life. ILC progenitors

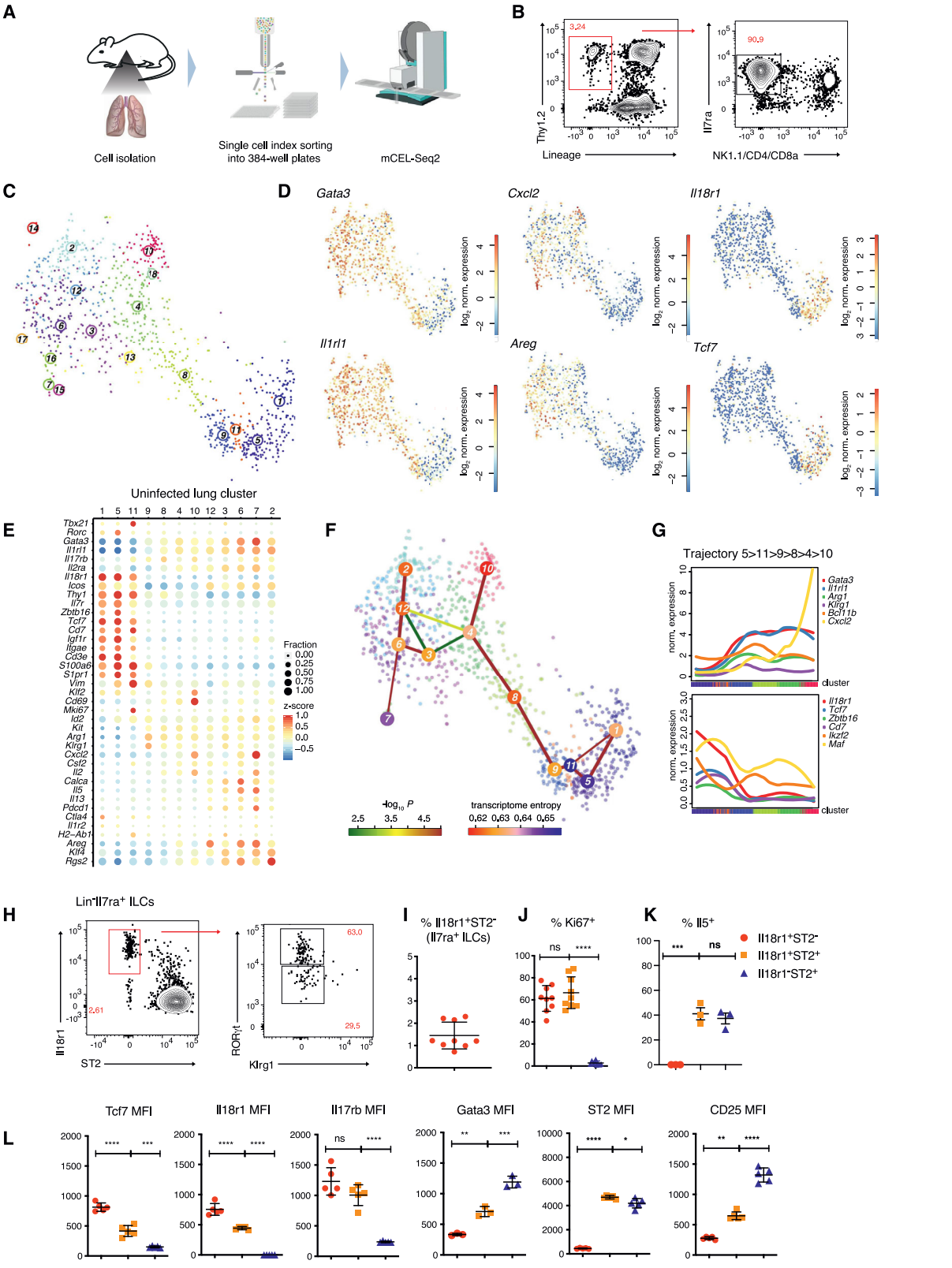

(legend on next page)

are present in human peripheral blood (Lim et al., 2017), and patients with inflammatory diseases have increased frequencies of circulating ILCs (for review, see Mazzurana et al., 2018). Local pools of tissue-ILCs may hence receive input from distant cellular sources during inflammation, and local changes in ILC subsets and abundance correlate with a number of inflammatory diseases (Mazzurana et al., 2018). Although murine ILC2s were found to traffic between organs during helminth infection (Gasteiger et al., 2015; Huang et al., 2018; Ricardo-Gonzalez et al., 2020), it remains unclear whether these cells have dedicated specialized functions and whether they are eventually recruited to replenish the local pool of resident cells. Thus, ILCs detected in a given tissue may be generated from different cellular sources and at different times during ontogeny. How the local pools of ILCs are being maintained and renewed is currently unknown. In particular, we lack a detailed understanding of the defined stages of differentiation of tissue ILCs, the phenotype of "immature" ILCs, as well as the sites and tissue niches where maturation occurs.

To address these questions, we generated a comprehensive single-cell atlas of ILC populations in the bone marrow (BM) and neonatal and adult lung at steady state, as well as during helminth infection in wild-type, parabiotic, and shield chimeric mice. Our findings identify local progenitors of tissue ILCs and highlight tissue adaptation and *in situ* differentiation as a mechanism of ILC maintenance and phenotypic diversification. In addition, the single-cell RNA sequencing (RNA-seq) datasets (http://murine-ilc-atlas.ie-freiburg.mpg.de/) represent an interactive resource for further exploration of ILC biology.

RESULTS

Heterogeneity of ILC2s in Healthy Lung Tissue

To characterize the full phenotypic spectrum of adult lung ILC2s in an unbiased manner, we fluorescence-activated cell sorting (FACS)-purified lineage-negative (Lin^-) $CD45^+Il7ra^+Thy1^{+/low}$ $NK1.1^-$ "pan-ILCs" for single-cell RNA sequencing (scRNA-seq), excluding natural killer (NK) cells and ILC1, but not ILC3, which are relatively rare in the lung (Figures 1A, 1B, and S1A). As committed ILC progenitors (ILCPs) and mature tissue ILCs express Il7ra (Constantinides et al., 2014; Klose et al., 2014), we expected that this sorting strategy samples the entire differentiation tree of ILC2s including putative early differentiation stages. Clustering cells using RaceID3 (Herman et al., 2018) yielded 12 clusters with >20 cells (Figure 1C). Except for clusters 1, 5, and 11, all cells highly expressed *Gata3* and *Il1rl1* (Figures 1D and 1E), which are markers of mature ILC2s in the lung. We detected different effector ILC2 sub-types such as cluster 10, with increased expression of the neutrophil recruiting factor *Cxcl2*, *Il2*, *Klf2*, and *Cd69*, or cluster 12, with elevated *Areg*, *Calca*, and *Csf2* levels (Figures 1D, 1E, and S1B). In addition, clusters 6 and 7 shared increased expression of *Cxcl2*, *Areg*, *Il13*, *Il5*, and *Calca*, but were distinct with regard to expression of *Calca* and *Csf2* versus *Il2*, *Cxcl2*, and *Pdcd1*, respectively. Besides these effector-like ILC2s resembling subsets of $ST2^+$ natural ILC2s (nILCs) (Nagashima et al., 2019; Wallrapp et al., 2017), we identified clusters 1, 5, and 11 characterized by low expression of *Gata3* and *Il1rl1*. Only a small fraction of cells in these clusters expressed low levels of ILC2 effector genes such as *Cxcl2*, *Areg*, and *Il13* or *Il5*. We also detected cells expressing *Rorc* and *Tbx21* within clusters 5 and 11, respectively (Figure 1E and S1C), indicating mixed lineage contributions as previously observed (Wallrapp et al., 2017). Few cells in clusters 1 and 5 expressed T cell markers *Cd3e* and *Trdc*, akin to reported subsets of murine and human ILCs (Björklund et al., 2016; Robinette et al., 2015), although a contamination of T cells with decreased surface CD3ε cannot be ruled out (Figure S1A). Interestingly, cells in clusters 1, 5, and 11 had increased levels of *Il18r1*, *Thy1*, *Cd7*, and *Tcf7*. The Notch target Tcf7 is expressed in ILCPs and CD7 in circulating human ILC precursors (Constantinides et al., 2014; Harly et al., 2019; Ishizuka et al., 2016; Lim et al., 2017). Of note, a subset of cells in clusters 1, 5, and 11 expressed *Zbtb16*, a marker of committed ILCPs (Ishizuka et al., 2016; Klose et al., 2014; Lim et al., 2017), and few of these cells co-expressed combinations of *Rorc*, *Tbx21*, and *Il17rb*, consistent with a mixed lineage-potential (Figure S1C). In addition, we observed elevated *Igfr1* in clusters 1 and 5, a receptor suggested to be critical for recently identified ILC3-progenitors in neonatal lung (Oherle et al., 2020).

To investigate if these cells represent early differentiation stages of tissue ILCs, we analyzed the developmental relationship of lung ILC subsets with StemID2, which connects related clusters to construct a lineage tree (Figure 1F). This analysis predicted a differentiation trajectory connecting $Il18r1^+Gata3^{lo}$ $Il1rl1^{lo}$ cells (clusters 1, 5, and 11) to ILC2s with increasing levels of *Il1rl1* and intermediate expression of effector cytokines

Figure 1. Heterogeneity of ILC2s in Healthy Adult Lung Tissue and Immature $Il18r1^+$ ILCs

(A) Workflow for lung ILC scRNA-seq library preparation.

(B) Representative sorting strategy for $Lin^-NK1.1^-Il7ra^+Thy1.2^{+/low}$ "pan"-ILCs from lung.

(C) T-distributed stochastic neighbor embedding (t-SNE) map of single-cell lung ILC transcriptomes clustered with RaceID3.

(D) t-SNE maps indicating log2 normalized expression of candidate genes.

(E) Candidate gene expression for clusters with at least 20 cells. Color represents *Z* score of the mean expression across clusters and dot size represents fraction of cells in the cluster expressing the gene.

(F) Lineage inference using StemID2. Node color depicts transcriptome entropy and link color indicates p value of StemID2 links ($p < 0.05$, STAR Methods).

(G) Pseudo-temporal gene expression profiles (local regression) of representative ILC2 genes (top) and ILC progenitor genes (bottom) along the predicted trajectory. Color bars indicate cluster identity.

(H and I) Representative FACS analyses of Lin^-Il7ra^+ ILCs in adult lung at steady state. Gating (H) and percentage (I) of $Il18r1^+ST2^-ROR\gamma t^-Klrg1^-$ ILCs.

(J and K) Fraction of $Ki67^+$ (J) and $Il5^+$ (K) cells within the indicated lung ILC subsets (ICS after incubation with monensin, $ROR\gamma t^+$ ILCs are not excluded).

(L) FACS analysis of Lin^-Il7ra^+ lung ILCs subdivided into $Il18r1^+ST2^-ROR\gamma t^-Klrg1^-$, $Il18r1^+ST2^+$, and $Il18r1^-ST2^+$ ILCs. Depicted are the mean fluorescence intensities (MFI) for Tcf7, Il18r1, Il17rb, Gata3, ST2, and CD25.

Data in (H)–(L) are representative of 2–3 independent experiments (n = 4–12 mice). Graphs in (I), (J), and (K) depict data as mean ± SD, (one-way ANOVA Tukey's multiple comparisons test, *$p < 0.05$, **$p < 0.01$; ***$p < 0.001$; ****$p < 0.0001$; ns, not significant).

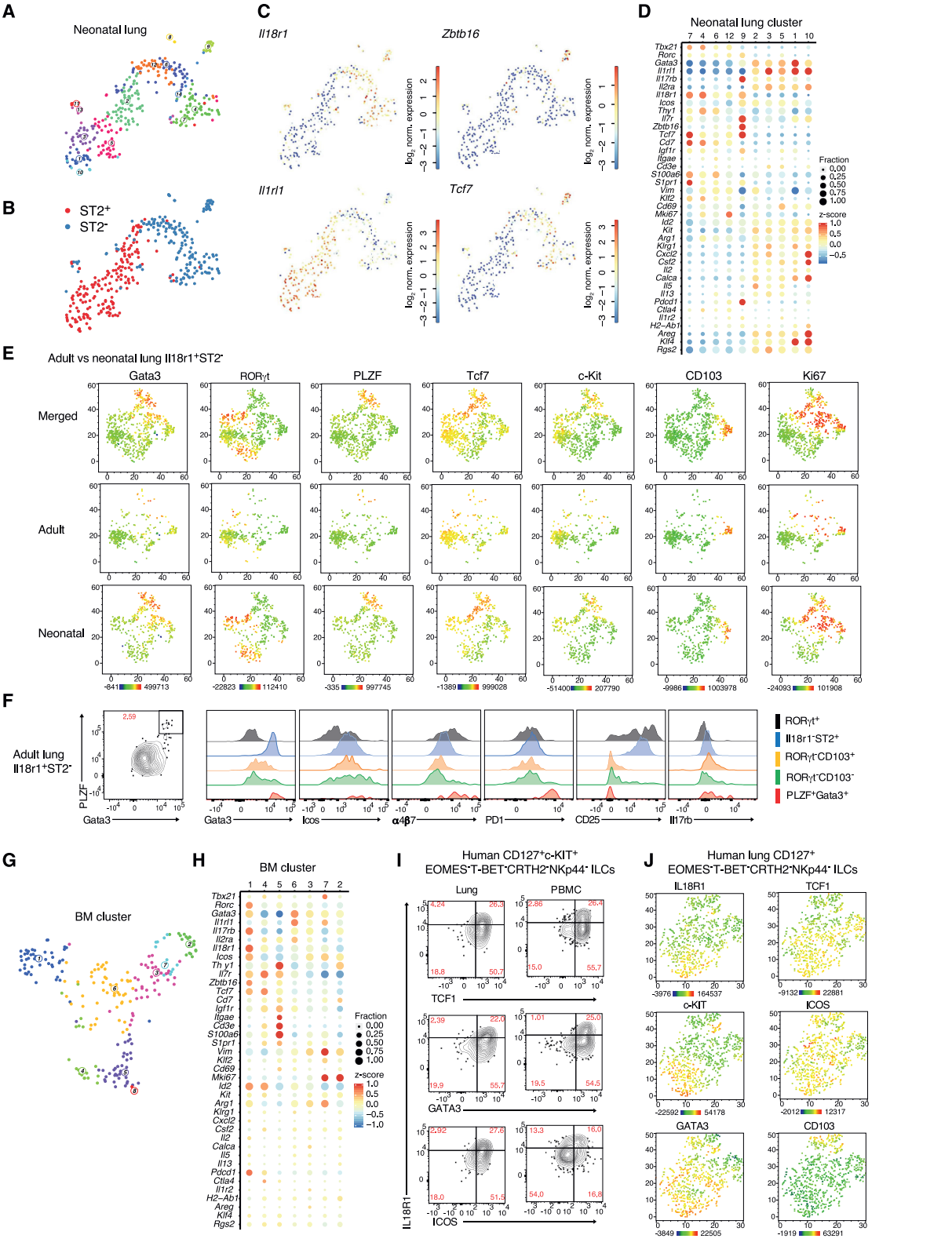

(legend on next page)

(clusters 9, 8, and 4) and to mature effector clusters (10, 12, 6, 7, and 2) (Figure 1F). Elevated transcriptome entropy for clusters 1 and 5 suggested a more naive state compared to the other clusters (Grün et al., 2016). After ordering cells along the trajectory starting at cluster 5 with the highest expression of known progenitor marker genes, and extending via clusters 11, 9, 8, and 4 toward cluster 10, pseudo-temporal gene expression profiles were grouped into distinct co-expression modules (Figures S1D and S1E; STAR Methods). Whereas the *Cxcl2*-expressing cluster 10 represents one possible endpoint of the trajectory, other mature clusters (2, 6, 7, and 12) correspond to alternative endpoints branching out from cluster 4 (Figure S1F).

Along the trajectory, we observed gradual increases of *Gata3*, *Il1rl1*, *Klrg1*, and *Bcl11b*, which have known functions in ILC2 differentiation (Califano et al., 2015; Yu et al., 2015). Concomitantly, expression of *Il18r1* and *Cd7* was decreased along with ILC progenitor genes such as *Zbtb16*, *Tcf7*, *Maf*, and *Ikzf2* (Figure 1G) (Harly et al., 2019; Ishizuka et al., 2016; Seehus et al., 2015). These inferred gene-expression dynamics suggested that mature *Gata3*^{hi}*Il1rl1*^{hi} ILC2s can differentiate from progenitor-like *Il18r1*$^{+}$*Gata3*^{lo}*Il1rl1*^{lo} ILCs (clusters 1, 5, and 11) in the lung. FACS analysis confirmed that Il18r1^{+}ST2^{-}RORγt^{-}Klrg1^{-} cells, hereafter referred to as Il18r1^{+}ST2^{-} cells, represented ~2% of Lin^{-}Il7ra^{+} ILCs (Figures 1H and 1I) and were also detected in lungs of T cell-deficient RAG$^{-/-}$ and TCRβδ$^{-/-}$ mice (Figure S1G and data not shown). Consistent with the gene signatures predicted for cluster 11 (Figure 1D), a high fraction of these cells was positive for the proliferation marker Ki67, suggesting their capacity for local expansion or self-renewal (Figure 1J). Together, these observations indicated that Il18r1^{+}ST2^{-} cells comprise immature differentiation stages of ILC2s that are enriched in the lung, where they may undergo local maturation. Consistently, when we analyzed lung ILC2s by dividing them into three subsets that were predicted to map successively along the inferred maturation trajectory (i.e., Il18r1^{+}ST2^{-}, Il18r1^{+}ST2^{+}, and Il18r1^{-}ST2^{+} cells), we found that cells decreased Ki67, Il18r1, Il17rb, and Tcf7 protein levels along this trajectory, while gaining expression of CD25, ST2, Gata3, and Il5 protein, which all characterize mature ILC2s in the lung (Figures 1J–1L).

To demonstrate that clustering and trajectory inference were not driven by proliferation associated programs, we removed proliferation associated genes prior to analysis (STAR Methods) and obtained a similar trajectory connecting *Il18r1*$^{+}$*Gata3*^{lo}*Il1rl1*^{lo} cells to effector-like ILC2s (Figures S1H–S1K). Together, these observations suggested that Il18r1^{+}ST2^{-} cells comprise early immature differentiation stages of ILC2s that are enriched in the lung, where they may locally mature.

Expression of *Il18r1*, *Tcf7*, and *Cd7* as well as effector genes *Il5*, *Il13*, and *Il17a* has recently been reported for ILC2s in the skin (Bielecki et al., 2018; Kobayashi et al., 2019; Ricardo-Gonzalez et al., 2018), raising the possibility that Il18r1^{+}ST2^{-} cells comprise heterogeneous ILC subtypes. To better characterize *Il18r1*$^{+}$ ILCs across tissues, we integrated our data with lung and skin single-cell transcriptomes from Ricardo-Gonzalez et al. (2018) and tested for the presence of discrete progenitor and effector states (Figure S2A; STAR Methods). We found that *Il18r1* expressing lung ILCs largely clustered separately from mature skin ILC2s expressing ILC2 effector genes (Figures S2A and S2B). However, a fraction of skin ILCs with increased *Igf1r*, *Tcf7*, *Zbtb16*, and *Pdcd1* expression clustered together with immature *Il18r1*$^{+}$ lung ILCs, suggesting an immature progenitor phenotype (Figures S2A–S2C). It is important to note that lung and skin-ILCs were sorted as Il5-mRNA-reporter^{+} cells by Ricardo-Gonzalez et al. (2018), and therefore this analysis may underestimate the frequency of progenitor-like cells. Reminiscent of these distinct phenotypes in skin, we detected CD103^{+}Il18r1^{+} cells in the lung, a fraction of which also expressed cytokines Il5, Il13, and Il17a upon *in vitro* re-stimulation (Figures S2D and S2E). These combined analyses revealed a previously unappreciated heterogeneity of Il18r1^{+}ST2^{-} ILC subtypes in skin and lung.

Il18r1^{+}ST2^{-} ILCs in Neonatal and Adult Lung Share Similarities with Il18r1^{+} ILC Progenitors in the BM

We next asked how the Il18r1^{+}ST2^{-} putative ILC2 progenitors from adult lung compare to known ILC progenitors. ILC2s are generated in different developmental windows during ontogeny, and cells emerging during neonatal life can persist in the adult lung (AL) (Schneider et al., 2019). To test whether corresponding progenitor populations are present in the neonatal lung (NL), we sequenced ST2^{+} and ST2^{-} ILCs from postnatal day 4 (P4) lung (Figure S3A) and performed clustering analysis (Figures 2A and 2B). Within the ST2^{-} compartment, cluster 9 exhibits a naive ILC signature akin to AL clusters 1, 5, and 11, with increased expression of *Il18r1*, *Tcf7*, *Zbtb16*, and *Pdcd1*, as well as intermediate levels of *Gata3* and high expression of *Il17rb* (Figures 2C and 2D), suggesting predominant ILC2 bias. Clusters 4, 6, 7, and 12 shared expression of *Il18r1* and *Tcf7*, and resembled

Figure 2. IL18r1^{+}ST2^{-} ILCs in Neonatal and Adult Lung Share Similarities with IL18r1^{+} BM ILCPs

(A–C) t-SNE maps of neonatal lung ILC single-cell transcriptomes highlighting RaceID3 clusters (A) or sorted ST2^{-} and ST2^{+} ILCs (B), and log2 normalized expression of representative genes marking putative ILC progenitors (C).

(D) Expression of candidate genes within neonatal lung clusters with at least 10 cells. Color represents *Z* score of the mean expression across clusters, and dot size represents fraction of cells in the cluster expressing the gene.

(E) FACS analysis of neonatal (P4) and adult (6–8 weeks) Il18r1^{+}ST2^{-} lung ILCs, represented as t-SNE maps, indicating expression levels for Gata3, RORγt, PLZF, Tcf7, c-Kit, CD103, and Ki67.

(F) Histograms comparing ILC subsets (PLZF^{+}Gata3^{+}, RORγt^{-}CD103^{-}, RORγt^{-}CD103^{+}, Il18r1^{-}ST2^{+} ILC2s, and RORγt^{+} ILC3) in adult lung for Gata3, Icos, α4β7, PD1, CD25, and Il17rb expression levels. Data are representative of 2–3 independent experiments (n = 6–12 mice).

(G) t-SNE map of Il18r1^{+}Icos^{+} BM ILCs highlighting RaceID3 clusters.

(H) Expression of candidate genes for Il18r1^{+}Icos^{+} BM clusters with at least 10 cells. Color represents *Z* score of the mean expression across clusters and dot size represents fraction of cells in the cluster expressing the gene.

(I and J) FACS analysis of human lung and PB ILCs pre-gated on CD45^{+}Lin^{-}CD127^{+}EOMES^{-}T-bet^{-}CRTH2^{-}NKp44^{-}c-KIT^{+} (I) or c-KIT$^{+/-}$ ILCs (J). Figures depict representative staining (I) and t-SNE maps (J) indicating the expression levels of selected markers. Data are representative of 3 independent experiments (n = 2–4 samples each).

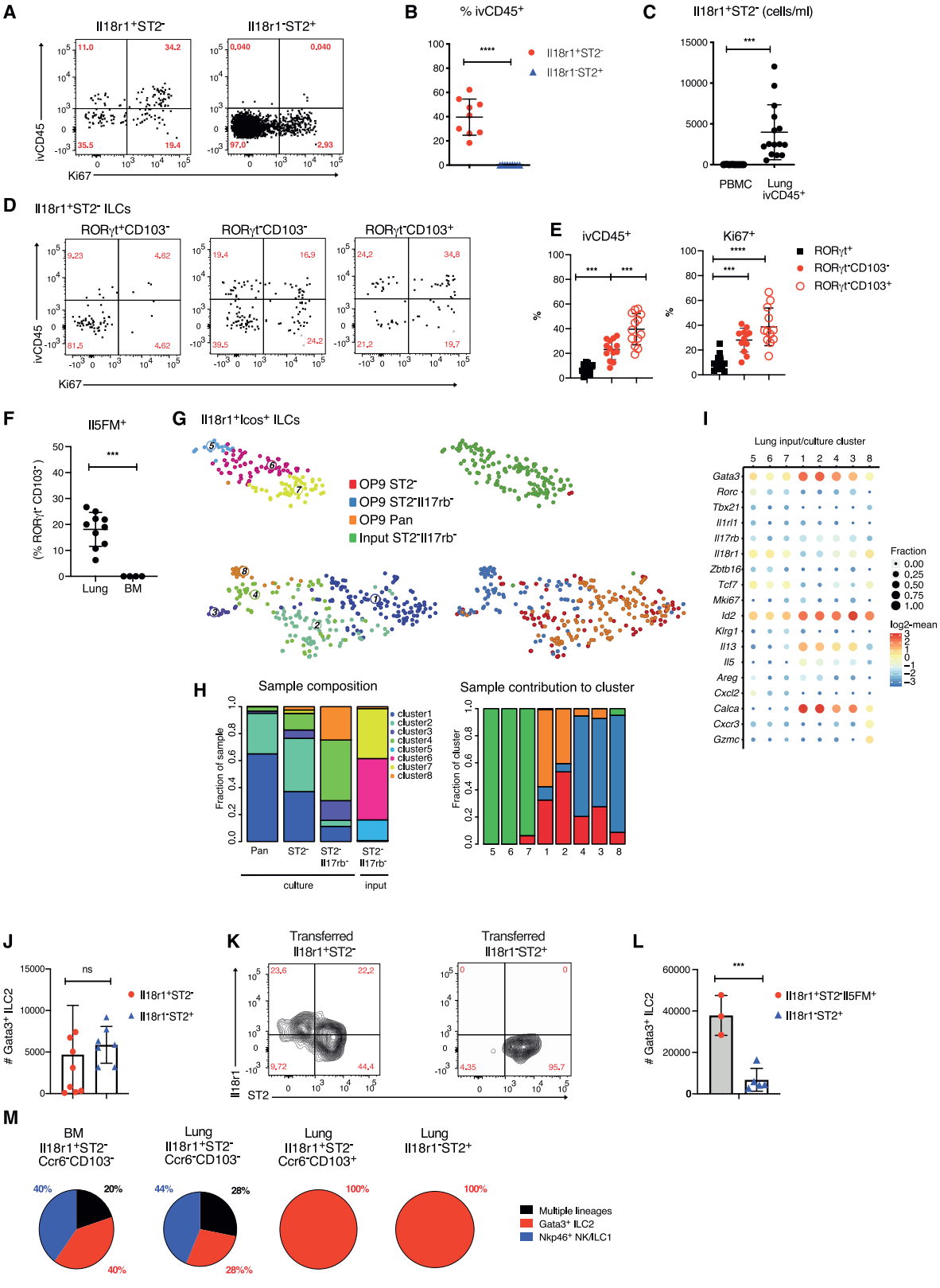

(legend on next page)

ILC1s or NK cells with expression of *Tbx21* (Figure 2D). FACS analysis confirmed the heterogeneity of Il18r1$^+$ ST2$^-$ cells and the presence of Il18r1$^+$Tcf7$^+$ cells that expressed Zbtb16 (PLZF), c-Kit, PD1, $\alpha4\beta7$, and Ki67 to variable degrees in both NL and AL (Figures 2E, 2F, and S3B–S3D). These cells shared expression of many genes with Il18r1$^+$Icos$^+$ BM ILCs that we further characterized by scRNA-seq (Figures 2G and 2H) and cells that have recently been defined as Id2$^+$ BM ILCPs (Xu et al., 2019). By integrating our data with published BM ILC scRNA-seq data (Walker et al., 2019), we confirmed that BM Il18r1$^+$Icos$^+$ cells contain ILCPs with ILC2 bias (Figures S3E–S3H). Accordingly, cells of Il18r1$^+$Icos$^+$ BM cluster 1 displayed increased expression of *Tcf7*, *Zbtb16*, *Pdcd1*, and *Il17rb* (Figure 2H), reminiscent of NL cluster 9. Although *Il18r1*$^+$ NL clusters lacked expression of *Cd3* genes, BM clusters 4 and 5, as well as AL progenitor clusters 1 and 5, expressed these genes. In addition, we resolved clusters 2 and 7 with increased *Mki67* expression (Figure 2H). These data confirmed the recently described phenotypic spectrum of BM ILC progenitors and revealed that corresponding populations with a similar heterogeneity exist in NL and AL (Figures 1 and 2A–2F). Circulating human ILC progenitors reminiscent of the populations we identified here were described recently (Lim et al., 2017). The IL7R$^+$ c-KIT$^+$ bulk population, which possibly include CRTH2$^-$ cells biased toward ILC2 lineage differentiation (Nagasawa et al., 2019) displays the transcriptional profile of *IL18R1*, *TCF7*, *CD7*, and *ZBTB16* (Lim et al., 2017). Because expression of these genes was not tested previously at the protein level, we analyzed human ILCs in peripheral blood and lungs and identified a population of IL7R$^+$ IL18R1$^+$TCF1$^+$ (encoded by the *TCF7* gene) cells that expressed GATA3 while lacking markers of mature NK cells, ILC1, ILC2, and ILC3 (i.e., EOMES, T-bet, CRTH2, and NKp44, respectively) (Figures 2I, 2J and S3I). Again, similar to cells in the murine lung, we observed graded expression of IL18R1, TCF1, GATA3, c-KIT, ICOS, and CD103, reminiscent of the described spectrum of murine Il18r1$^+$ ILCs in neonatal and adult lungs and BM ILCPs (Walker et al., 2019; Xu et al., 2019).

Together, these observations raised the possibility that we have identified a murine counterpart to ILC progenitors present in human lungs, reinforcing the question about the developmental potential of these cells.

Il18r1$^+$ ILCs Comprise Immature Cells that Give Rise to Gata3^{hi} ILC2s in the Lung

Consistent with the detection of human ILCPs in peripheral blood, we have previously observed rare donor-derived cells among BM ILCPs in parabiotic mice, suggesting that ILCPs, similar to HSCs, can physiologically traffic and systemically disperse at low levels in adult mice (Gasteiger et al., 2015; Wright et al., 2001). Of note, around 30%–40% of Il18r1$^+$ST2$^-$ cells were labeled with intravenously injected anti-CD45 (ivCD45) (Figures 3A and 3B), and expressed genes associated with migration such as *Vim* and *S1pr1* (cluster 11, Figure 1E), and therefore could represent cells transiting through the pulmonary circulation. Il18r1$^+$ST2$^-$ cells were, however, extremely rare in the peripheral blood but readily detected in the ivCD45$^+$ fraction of the lung (Figure 3C), indicating that they may marginalize and enrich in lung vasculature. Interestingly, although Il18r1$^+$ ILCs comprised a high fraction of ivCD45$^+$ and Ki67$^+$ cells, the majority of them were still ivCD45$^-$, indicating their presence in the lung tissue at steady state (Figures 3D and 3E). Consistent with their residency in the lung and a minor exchange with circulating cells, all ivCD45$^-$Il18r1$^+$ST2$^-$ subtypes were predominantly host-derived in parabiotic mice (Figure S4A). In addition, when comparing cells with an ILCP phenotype (Il18r1$^+$ST2$^-$CD103$^-$ RORγt$^-$) in lung versus BM, we found that ~20% fate-mapped positive for Il5 in lungs but not in the BM of Il5-Cre mice, further indicating that they were distinct from BM ILC progenitors "in transit" (Figure 3F). Instead, these data support the idea that ILCPs gained *Il5* expression locally and matured toward ILC2s within the lung tissue.

To directly test their cell-intrinsic differentiation potential, we purified Il18r1$^+$Icos$^+$ lung ILCs by FACS for *in vitro* differentiation assays. In order to deplete cells that may be committed toward the ILC2 lineage, we additionally sorted ST2$^-$ and ST2$^-$Il17rb$^-$ double negative Il18r1$^+$Icos$^+$ ILCs from adult lungs and cultured all three populations on OP9 in the presence of Il2, Il7, Il1β, and Il23 (Figure S4B), conditions that were recently used to expand

Figure 3. Il18r1$^+$ ILCs Are Immature Cells that Give Rise to Gata3^{hi} ILC2s in the Lung

(A and B) FACS analysis of Ki67 expression and intravenous CD45 label (ivCD45) in Il18r1$^+$ST2$^-$RORγt$^-$Klrg1$^-$ and Il18r1$^-$ST2$^+$ adult lung ILC2s. Representative gating (A) and percentage of ivCD45$^+$ cells within indicated ILC subsets (B).

(C) Number of Lin$^-$Il7ra$^+$Il18r1$^+$ cells per mL blood in PBMCs (Il18r1$^+$ST2$^-$ ILCs) and lung (ivCD45$^+$Il18r1$^+$ST2$^-$RORγt$^-$Klrg1$^-$ ILCs). Graphs in (B) and (C) depict data as mean ± SD (unpaired t test, *p < 0.05, **p < 0.01; ***p < 0.001; ****p < 0.0001; ns, not significant).

(D and E) Representative gating (D) and percentage of Ki67$^+$ and ivCD45$^+$ cells (E) for indicated Il18r1$^+$ST2$^-$ ILC subsets in adult lung. Data are pooled from 3–4 independent experiments (n = 4–16 mice).

(F) Percentage of Il5^{Cre} fate-mapped (Il5FM$^+$) Il18r1$^+$ST2$^-$RORγt$^-$CD103$^-$ ILCs in lung and BM. RORγt staining was used to exclude ILC3. Data are pooled from 2–3 independent experiments (n = 4–9 mice). Graphs in (E) and (F) depict data as mean ± SD (one-way ANOVA Tukey's multiple comparisons test (E) or unpaired t test (B, D, and F), ***p < 0.001; ****p < 0.0001). Data are pooled from 3–4 independent experiments with a total of n = 8–15 mice).

(G) t-SNE representation of single-cell transcriptomes of lung Il18r1$^+$Icos$^+$ ILCs before ("input") and after culture ("output") highlighting RaceID3 clusters.

(H) Cluster composition of samples (left) and normalized sample composition of clusters (right, for legend see G).

(I) Expression of candidate genes for input and output populations. Color represents log2 mean expression in the respective cluster and dot size indicates fraction of cells expressing the gene in the cluster.

(J) Total number of Gata3$^+$ ILC2s after culture of indicated lung ILCs for 15 days in the presence of Il2, Il7, SCF, Il25, and Il33 on OP9-DL1.

(K) FACS analysis of Lin$^-$Il7ra$^+$ lung ILCs on d21 post transfer into sublethally irradiated CD45.2$^+$RAG$^{-/-}\gamma c^{-/-}$ mice. Congenically marked Il18r1$^+$ST2$^-$ and Il18r1$^-$ST2$^+$ ILCs sorted from lungs of d2 Nb infected mice were cotransferred (2,000 cells each). Data are representative of 2 individual experiments (n = 3 mice).

(L) Total number of Gata3$^+$ ILC2 after culture of indicated lung ILCs as in (J). Data in (J) and (L), are pooled from 2 independent experiments with n = 3–4 repeat wells each.

(M) Indicated lung and BM ILC subsets were sorted as single cells onto OP9-DL1 monolayers and cultured for 19 days. Clonal progeny was analyzed by FACS. Pie charts indicate distribution of culture output across positive single cell cultures.

human ILCPs (Lim et al., 2017). After ~21 days, we performed scRNA-seq of lineage-negative output from these cultures along with the Il18r1$^+$Icos$^+$ST2$^-$Il17rb$^-$ input population. First, we confirmed that the input population co-clustered with the naive population from the uninfected lung ILC dataset and expressed only very low levels of *Il1rl1* and *Il17rb* (Figures S4C and S4D). Next, a combined analysis yielded 8 clusters, of which 5 corresponded to cells harvested from the culture (clusters 1, 2, 3, 4, and 8) and 3 represent the input population (clusters 5, 6, and 7) (Figures 3G and 3H). Clusters 1 and 2 are marked by the expression of *Il5* and high levels of *Gata3*, *Il13*, and *Calca* (Figure 3I) and were thus classified as ILC2s. The majority of cells differentiating from Il18r1$^+$Icos$^+$ and Il18r1$^+$Icos$^+$ST2$^-$ input populations gave rise to these ILC2s (95 and 77%, respectively), whereas only ~15% of cells originating from Il18r1$^+$Icos$^+$ST2$^-$Il17rb$^-$ cells were ILC2s in clusters 1 and 2. Instead, these cells predominantly (61%) populated clusters 3 and 4, comprising a mixture of ILC2s and ILC3s with reduced levels of ILC2-specific gene expression. Approximately 25% of cells originating from the Il18r1$^+$Icos$^+$ST2$^-$Il17rb$^-$ population gave rise to NK/ILC1 cluster 8 characterized by expression of *Cxcr3*, *Klrk1*, and *Gzmc*. Furthermore, whereas ILC2s largely reduced or lost *Il18r1* and *Tcf7* expression, cells in cluster 8 maintained high expression of these genes (Figure 3G-I). Of note, only a small fraction of cluster 8 originated from cultured Il18r1$^+$Icos$^+$ST2$^-$ cells (Figure 3H), suggesting that depletion of Il17rb-expressing cells enriched the fraction of cells with ILC1/NK cell potential. We also assessed the potential of the Il18r1$^+$Icos$^+$ counterparts from the BM in the same conditions. Consistent with lung ILCs, the majority of Il18r1$^+$Icos$^+$ST2$^-$ BM ILCs gave rise to ILC2s. In contrast, Il18r1$^+$Icos$^+$ST2$^-$Il17rb$^-$ cells from the BM gave rise to only very few *Il13* expressing ILC2s (Figures S4E and S4F). Of interest, the presence of Il18 in these cultures led to the increased expression of ILC2 effector genes (Figures S4H and S4I), as recently suggested (Ricardo-Gonzalez et al., 2018), but did not change the expansion of Il18r1$^+$ ILC2s *in vitro* (Figure S4J).

These data suggested that Il18r1$^+$ lung and BM ILCs predominantly differentiated into *Gata3*^{hi}*Il13*$^+$ ILC2. This bias toward ILC2s was evident under culture conditions that were recently shown to expand ILC progenitors (Lim et al., 2017) in the absence of alarmins Il25 and Il33, known to enforce ILC2 development. In order to test the expansion potential under such ILC2-activating conditions, we cultured Il18r1$^+$ST2$^-$ and Il18r1$^-$ST2$^+$ ILC2s from lung in the presence of Il25 and Il33 and found that both populations generated similar numbers of Gata3^{hi} ILCs as ST2$^+$ cells (Figure 3J). To test the differentiation potential *in vivo*, we activated the ILC2 compartment through infection with the parasitic helminth *Nippostrongylus brasiliensis* (Nb), which induces the local expansion of ILC2s. To this end, we sort-purified Il18r1^{+-}ST2$^-$ and Il18r1$^-$ST2$^+$ ILCs from lungs 2 days (d) post infection (p.i.) and co-transferred cells at a 1:1 ratio into sublethally irradiated RAGγc$^{-/-}$ hosts, as previously established (Ghaedi et al., 2020; Xu et al., 2019). Three weeks after transfer, we found that Il18r1$^+$ST2$^-$ cells partly gave rise to Il18r1$^+$ST2$^-$, Il18r1$^+$ST2$^+$, and Il18r1$^-$ST2$^+$ ILC2s, consistent with the idea that these cells can differentiate into mature ILC2s (Figure 3K). Transferred Il18r1$^-$ST2$^+$ ILC2s, in contrast, only generated Il18r1$^-$ST2$^+$ progeny, suggesting that Il18r1$^+$ cells represent early stages on the differentiation trajectory that are not readily generated from more mature cells in lymphopenic recipients.

Notably, Il18r1$^+$ cells are a mixture of Ccr6$^+$RORγt$^+$ ILC3s (Figure S4K) as well as Ccr6$^-$RORγt$^-$ immature cells with NK/ILC1 and ILC2 potential, as suggested by the differentiation of these cells *in vitro* and *in vivo*, upon transfer (Figures S4K–S4M). Therefore, only a fraction of the sorted Il18r1$^+$ subsets likely represented cells with ILC2 fate. To enrich for these cells, we sorted Il18r1$^+$ST2$^-$Il5FM$^+$ cells for culture in the presence of Il25 and Il33, yielding many more Gata3^{hi} ILC2s than culture of ST2$^+$ cells, highlighting the unique expansion potential of these immature lung ILCs (Figure 3L). Consistently, transfer of Ccr6$^-$ cells (i.e., RORγt-depleted and ILCP-enriched cells) engrafted better and generated more ILC2s as compared to ST2$^+$ mature ILC2s *in vivo* (Figure S4M). To compare the clonal developmental potential of lung Il18r1$^+$ST2$^-$ subsets and BM ILCPs, we performed single-cell cultures in Il2, Il7, and SCF in the presence of Il25 and Il33. Intriguingly, we found that both Il18r1$^+$ST2$^-$CD103$^-$Ccr6$^-$ lung and BM ILCPs gave rise to ILC2 or ILC1/NK cells or multiple lineages (Figure 3M). CD103$^+$ and ST2$^+$ cells, in contrast, preferentially generated ILC2s, and ILC3s were undetectable under these type-2 polarizing conditions. Together, these data demonstrate that similar to the BM, the lung hosts a spectrum of immature cells with mixed lineage ILC potentials, including cells that are primed for ILC2 fate.

Emergence of ILC2 Subset Heterogeneity during *N. brasiliensis* Infection

Next, we investigated how the spectrum of phenotypic states of lung ILC2s and their differentiation trajectories change upon immune challenge. Infection with Nb causes local expansion of tissue-resident ILC2s during the acute phase of infection (Figure 4A), and around d15 postinfection (p.i.), in the tissue-repair phase, a fraction of lung ILC2s has emerged from cells recruited through the blood circulation (Gasteiger et al., 2015; Huang et al., 2018). During inflammation, ILCs exit from the small intestine (Huang et al., 2018), the lung (Ricardo-Gonzalez et al., 2020), and the BM (Stier et al., 2018) into the peripheral blood, and, hence, ILCs of different origins can traffic to the lung during infection to extend the local spectrum of phenotypes and functions. In order to dissect the heterogeneity of lung ILC2s upon immune challenge, "pan-ILCs" were sequenced at different time points p.i. along with "pan-ILCs" from the peripheral blood and ivCD45$^+$ ILCs from the lung vasculature (Figure 4B). After combining with the uninfected lung data (Figure 1) and removal of NK cell and macrophage contaminations, we inferred ILC2 sub-types using RaceID3 (Figure 4C). Our analysis highlights the dynamic emergence of ILC heterogeneity and specialization over time (Figures 4D and S5A). For example, cells from the uninfected condition contributed mainly to clusters 9, 11, 12, and 20 and *Il18r1*$^+$ immature ILCs from the uninfected condition predominantly mapped to cluster 12 (Figures 4E, S5B, and S5C). ILC2s derived from d4 p.i. expressed high levels of *Calca*, *Csf2*, and *Cxcl2* and resided in clusters 4 or 10 together with a subset of ILC2s from the uninfected condition. However, ILC2s became more specialized during infection, exemplified by cluster 23 comprising almost exclusively d4 cells (Figures 4E and S5B), with marked expression increase of *Csf2*, *Cxcl2*, *Cxcl1*, and *Il5*, which promote neutrophil and eosinophil recruitment,

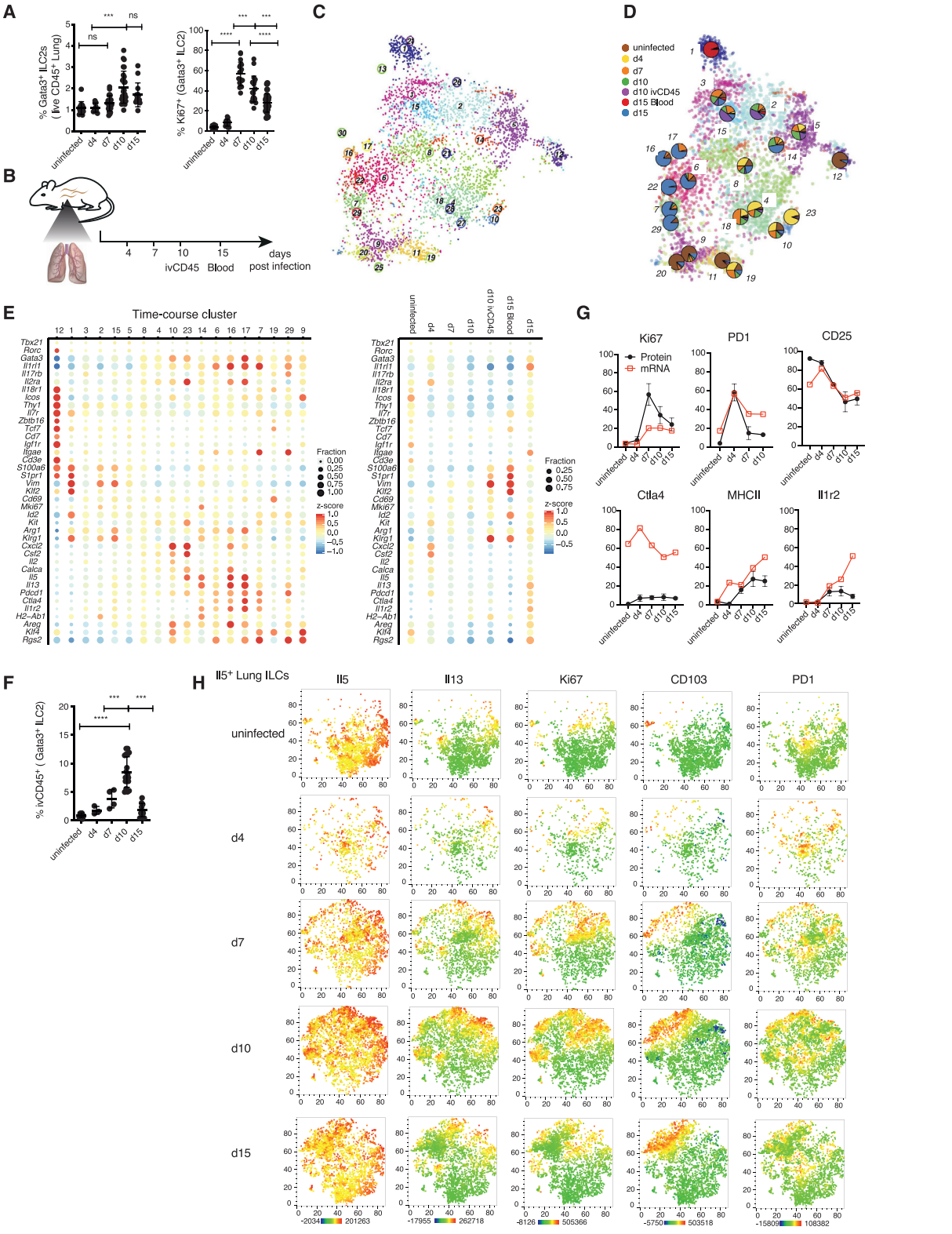

(legend on next page)

two myeloid subsets that expand in tissues early during helminth infection (Motran et al., 2018). Similarly, ILC2s isolated at d15 p.i. comprised a variety of different effector subsets, e.g., cluster 14 with high expression of MHCII complex genes *Cd74*, *H2-Ab1*, and *H2-Aa* (Oliphant et al., 2014; Symowski and Voehringer, 2019) and genes associated with T cell regulation such as *Il1r2*, *Ctla4*, and *Furin*, or clusters 16 and 17, expressing high levels of *Il5*, *Il13*, *Cxcl2*, and *Areg* (Figures 4E and S5B).

ILCs isolated on d7 and d10 p.i. contributed predominantly to clusters 2, 5, and 15, exhibiting enhanced expression of *Vim* and decreased expression of *Il1rl1*. Clusters 2 and 15 additionally had increased *Klrg1* expression (Figure 4E). We performed ivCD45 labeling to identify ILC2s that circulate through the lung during infection (Huang et al., 2018; Ricardo-Gonzalez et al., 2020) and sequenced ivCD45$^+$ cells on d10 p.i. when their frequency peaked at ~10% of all lung ILC2s (Figure 4F). IvCD45$^+$ ILC2s clustered mainly with d7 and d10 ILCs (clusters 2 and 15) and few ivCD45$^+$ cells also clustered with mature effector ILC2s (e.g., clusters 6, 7, and 23). In contrast, blood ILC2s sorted on d15 p.i., when the wave of tissue-exiting ivCD45$^+$ cells has largely ceded, constitute a separate cluster (cluster 1) with high expression of *Vim*, *Klrg1*, *Id2*, *Klf2*, and *S1pr1*, and have only minor contributions to clusters 2 and 3 (Figures 4D, 4E, and S5B). Among them we detected a tiny population of cells expressing *Il18r1*, *Icos*, *Tcf7*, and low levels of *Il1rl1*, consistent with the idea that Il18r1$^+$ST2$^-$ cells may traffic to the lungs where they enrich in the lung vasculature and in the tissue (Figures 3A–3C, S5D, and S5E).

We validated the dynamic regulation of selected markers, including PD1, MHCII, Il1r2, Ctla4, and CD25, on the protein level during the course of infection by flow cytometry, suggesting a close correlation of mRNA and protein levels for most genes (Figure 4G). Consistently, our analyses confirmed the regulated co-expression of Il1r2, PD1, and MHCII during late stages of infection (Figure S5F). Furthermore, we could validate the dynamic emergence of heterogeneous Il5-expressing ILC2s, co-expressing Il13 and/or PD1, resembling cluster 23 at d4 and clusters 16 and 17 at d10/d15 p.i. (Figure 4H).

Differentiation Trajectories of Lung ILC2s during *N. brasiliensis* Infection

We then investigated the differentiation dynamics of ILC2 subsets during Nb infection. Initially, we highlighted the position of cells from the early part of uninfected lung trajectory (uninfected lung clusters 1, 5, 11, 9, and 8 in Figure 1) in the combined dataset (Figure 5A). Cells of the uninfected lung cluster 1 were largely localized to cluster 12, which was dominated by cells from the uninfected condition (Figure S6A). In contrast, the majority of cells from uninfected lung clusters 5, 11, and 9, representing early ILC2 differentiation stages, mixed with cells isolated during infection in clusters 2 and 5 (Figure 5A), raising the question of whether these cells may undergo dynamic differentiation and give rise to mature effector ILC2s during Nb infection. We applied StemID2 to infer potential trajectories starting from *Il18r1*$^+$ immature ILCs in either cluster 5 or 12 and ending in mature ILC2 effector clusters such as cluster 16 or 23 (Figure 5B). A large fraction of immature uninfected lung cells localized to clusters 2 and 8, suggesting that differentiating immature *Il18r1*$^+$ ILCs transition through these stages. From cluster 8, the trajectory branched out, potentially terminating in early (d4) or late (d15) effector clusters 23 or 16, respectively (Figure 5B). Because the link between clusters 12 and 5 was populated well with intermediate single-cell transcriptomes (Figure S6B), we chose cluster 12 as a starting point, traversing cluster 5. Along both trajectories, we detected increased expression of *Arg1*, *Klrg1*, *Gata3*, *Il1rl1*, and effector cytokines, as well as decreased levels of ILC progenitor genes (Figure 5C). Of note, we detected cells expressing *Il18r1* and *Tcf7* also within mature ILC2 compartments, albeit at reduced levels and frequencies compared to the progenitor cluster 12 (Figures 4E and S6C). The cluster composition along the trajectory suggested the presence of alternative starting points. Cluster 2 or 15, marked by a high contribution of potentially infiltrating ivCD45$^+$ cells (Figure 5B), may represent such alternative starting points for the *in situ* differentiation into mature nILC2 effector cells, consistent with the observation that both recruited and resident cells can contribute to lung ILC2s (Figure S6D) (Gasteiger et al., 2015; Huang et al., 2018).

These observations suggested that lung ILC2s can differentiate from an *Il18r1*$^+$ *Tcf7*$^+$ immature population during Nb infection. We found that Il18r1$^+$ST2$^-$ cells were maintained during Nb infection while the proportion of ivCD45$^-$ cells among them gradually increased, consistent with the local expansion of these cells in the lung tissue (Figure 5D). At the same time, we observed a dramatic increase in highly proliferative Il18r1$^+$ST2$^+$ cells over the course of infection (Figure 5E), which we characterized as differentiation intermediates along an expression gradient of Tcf7 and Gata3 and that were generated *in vivo* from transfers of Il18r1$^+$ST2$^-$ immature cells (Figure 3K). Consistently, we observed the increase of ST2, Il5, Il13, and Ki67 within Il18r1$^+$ lung ILC2s over the course of infection (Figure 5F).

Figure 4. Emerging Heterogeneity of Lung ILC2s during *Nippostrongylus brasiliensis* Infection

(A) FACS analysis of the fraction of Lin$^-$Gata3$^+$ ILC2s among live CD45$^+$ cells (left) and of Ki67$^+$ cells among Lin$^-$Gata3$^+$ ILC2s (right) in Nb infected lungs. Data are pooled from 3 independent experiments with a total of n = 12–16 mice per time point.

(B) Sequenced samples at the respective time points during Nb infection.

(C) t-SNE map of combined Nb infection time course and uninfected lung data (cf. Figure 1) highlighting RaceID3 clusters.

(D) Overlay of t-SNE map from (C) with pie charts indicating normalized sample contribution to clusters.

(E) Expression of candidate genes for ILC subsets for inferred time-course clusters with at least 20 cells (left) or the respective sample (right). Color represents *Z* score of the mean expression across clusters/samples and dot size represents fraction of cells positive for the gene in the cluster/sample.

(F) Time course FACS analysis of the fraction of ivCD45$^+$ ILC2s in Nb infected lungs. FACS data are pooled from 2–3 independent experiments with n = 6–12 mice per time point.

(G) Time course FACS analysis of Il7ra$^+$ ILCs in Nb infected lungs (black) compared with fractions of RNA expressing cells of time course dataset (red). FACS data are pooled from 2–3 independent experiments with n = 6–9 mice per time point.

(H) Time course FACS analysis of Nb infected lungs. Expression of indicated markers represented as t-SNE maps for Il5$^+$ ILCs. Intracellular staining (ICS) after incubation with PMA, ionomycin, and monensin. Data are pooled from 5 mice for each time point and merged from equal numbers of Lin$^-$Il7ra$^+$ ILCs. Graphs in (A) and (F) depict data as mean ± SD (one-way ANOVA Tukey's multiple comparisons test, ***$p < 0.001$; ****$p < 0.0001$).

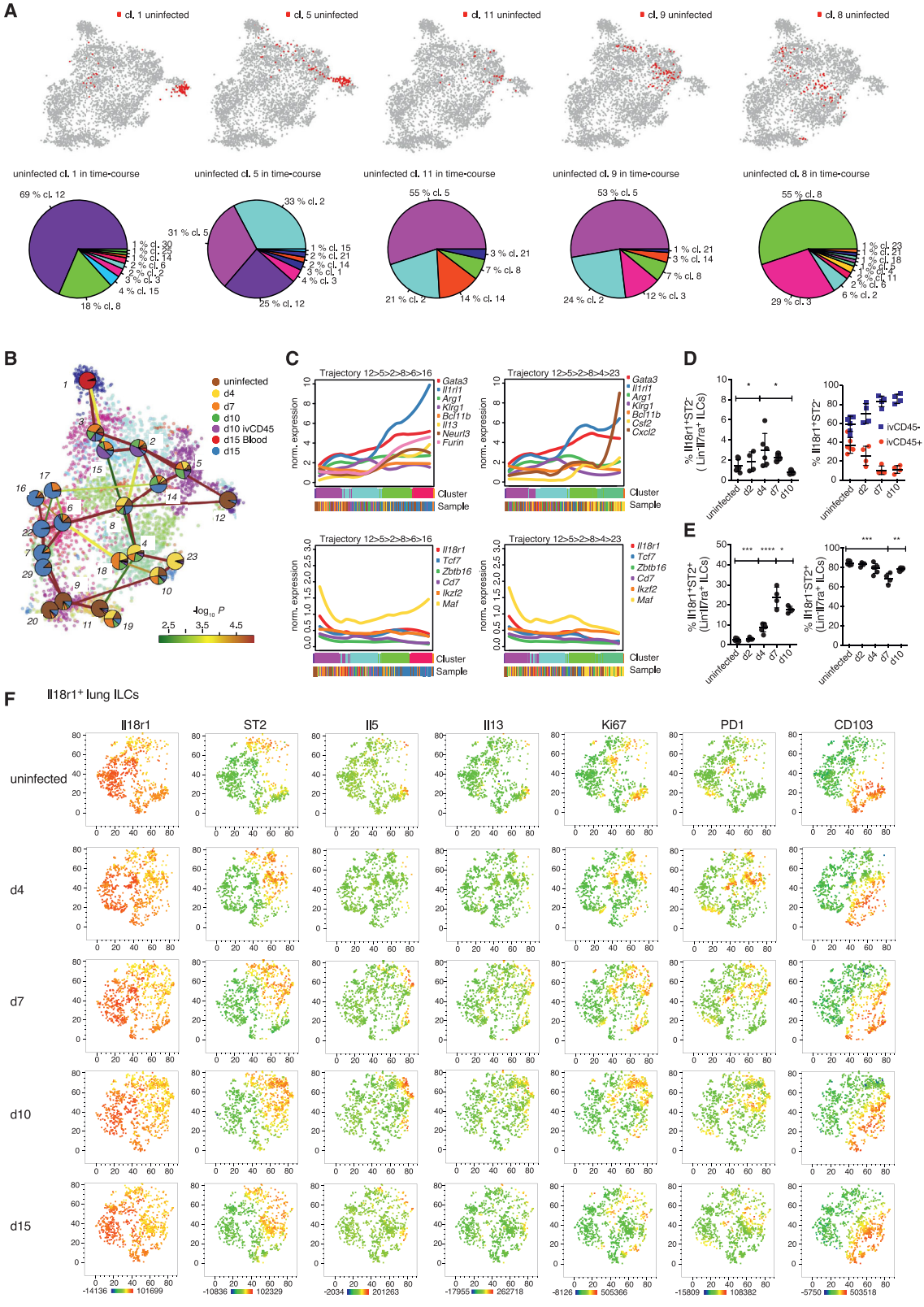

(legend on next page)

Recruited Cells Contribute to the Entire Phenotypic Spectrum of Lung ILC2s during *N. brasiliensis* Infection

A major open question is how cells recruited during inflammation contribute to the local pool of tissue ILCs, particularly, whether these cells retain specific phenotypes and functions or adapt to their new tissue-environment. To address this question, we analyzed infiltrating versus resident ILC2s from lungs of Nb-infected parabiotic mice. Here, two mice establish a common blood circulation, and infiltrated donor-derived cells can be identified through allogeneic markers. Parabionts were infected with Nb, and similar numbers of donor and host ILC2s were sorted for scRNA-seq on d15 p.i., a time point when donor-derived, i.e., recruited, ILC2s represent ~10%–15% of all lung ILC2s (Gasteiger et al., 2015; Huang et al., 2018). After RaceID3 analysis (Figure 6A), clusters were examined for their normalized host and donor contributions. Remarkably, all inferred clusters showed contribution of both host- and donor-derived cells (Figure 6B), with few differentially expressed genes between donor and host cells of the same cluster (Figure 6C). This observation demonstrated that cells recruited into the lung post parabiotic surgery contribute to all subpopulations that can be discriminated by unbiased scRNA-seq analysis at late stages of Nb infection.

Consistent with the idea of *in situ* differentiation of recruited cells from immature ILC2s, we found that some clusters were significantly enriched either for donor cells (clusters 3, 4, 5, 11, and 17) or host cells (cluster 1, 6, 7, 12, 13, and 15) (Figures 6B and S7A). Whereas the former exhibited the signature of immature ILC2s with high levels of *Il18r1*, *Tcf7*, and *Cd7*, and low levels of *Gata3* and *Il1rl1* (clusters 4, 11, and 17), the latter showed expression of *Calca* and cells of clusters 12 and 13 additionally increased expression of *Cxcl2*, *Areg*, and *Il5* (Figures 6D, 6E, and S7B). Thus, donor-derived cells are enriched in early differentiation stages. To further test this, we mapped the position of the donor- and host-enriched parabiosis clusters along the inferred trajectory of the time course data (Figure 5B; STAR Methods). The *Il18r1*$^{+}$ donor-dominated clusters 4, 11, and 17 of the parabiosis dataset had indeed the highest similarity to cells of time course cluster 12, marking one of our inferred origins of ILC2 differentiation during Nb infection. Conversely, clusters enriched for host-derived cells predominantly exhibited highest similarities with the terminal clusters of the inferred trajectories from the time course data (Figures 6F and S7C).

These results demonstrated that donor-derived recruited cells populate all clusters while being enriched in immature Il18r1^{+} ST2^{-} ILCs, consistent with their *in situ* differentiation and their potential role in the renewal of tissue ILC2s. Importantly, our analyses revealed that ILCs recruited into the adult lung can generate the entire spectrum of tissue ILC2s based on their single cell transcriptomes.

BM-Derived ILCs Give Rise to the Full Phenotypic Spectrum of ILC2s in the Adult Lung

We demonstrated that ILCs entering from the circulation give rise to all subtypes of tissue ILC2s during Nb infection (Figure 6B). However, the infiltrating cells can originate from different sources, including the BM (Constantinides et al., 2014; Klose et al., 2014; Stier et al., 2018), a circulating ILCP (Lim et al., 2017), or cells exiting from inflamed tissues (Huang et al., 2018; Ricardo-Gonzalez et al., 2020). These observations raise the possibility that cells from different origins give rise to limited specialized subsets of ILCs, and only together compose the full spectrum of tissue ILCs. Therefore, we investigated whether cells originating from a defined source contribute to specialized subsets, or whether they can reconstitute the full phenotypic spectrum of lung ILC2s. To this end, we adapted a shield chimera model (Gentek et al., 2018), where partial BM chimerism was established through transfer of BM after local irradiation of the hind legs (Figure 7A). Most of the body, including the lung, was shielded from the irradiation to avoid perturbation of the host tissue and immune cells. This procedure led to partial chimerism of BM-dependent cells of the myeloid and lymphoid lineages (e.g., NK cells), whereas very few ILC2s were detectable in the lung (Figure 7B). In contrast, ILC2s readily emerged from engrafted BM when shield chimeras were generated during the neonatal time window (data not shown), consistent with the local expansion of lung ILC2s during that time of ontogeny (Huang et al., 2018; Saluzzo et al., 2017; Schneider et al., 2019).

To test the differentiation potential of BM-derived cells in adult mice, adult shield chimeras were infected with Nb, and donor and host ILCs were sequenced on d15 p.i. (Figure 7A). Donor derived cells comprised ~5%–8% of lung ILCs (data not shown). Similar to our observations in parabiotic mice, all inferred clusters comprised both host and donor-derived cells (Figures 7C–7E). Again, we detected donor-enriched clusters with immature ILC2 signature expressing *Il18r1*, *Tcf7*, and *Zbtb16* (clusters 16 and 17) (Figures 7E, 7F, S7D, and S7E). Within-cluster comparison revealed reduced levels of *Ccr2*, *Ctla2a*, *Cxcl2*, and *Areg*, and higher levels of *Lmo4*, *Icos*, and *Il17rb* in donor versus host-derived cells (Figure 7G). These small, but consistent, differences suggested that donor-derived cells carry a signature

Figure 5. Differentiation Trajectories of Lung ILC2s during *Nippostrongylus brasiliensis* Infection

(A) t-SNE maps showing the distribution of uninfected lung immature clusters (cf. Figure 1) within the combined dataset (top) and pie charts of the distributions (bottom) (cf. Figure 4C).

(B) StemID2 lineage inference and normalized sample contribution to clusters depicted as pie-charts. Link color indicates p value of StemID2 links ($p < 0.05$, STAR Methods).

(C) Pseudo-temporal gene expression profiles (local regression) along depicted trajectories. Color bars indicate cluster and sample identity, respectively, of cells ordered along the depicted trajectory by StemID2.

(D) Time course analysis for the percentage of Il18r1^{+}ST2^{-}RORγt^{-}Klrg1^{-} ILCs (left), and the comparison of ivCD45-labeled and ivCD45-unlabeled fractions (right).

(E) Time course analysis for the percentage of Il18r1^{+}ST2^{+} (left) and Il18r1^{-}ST2^{+} (right) ILC2s. Data in (D) and (E) are representative of 2 independent experiments with n = 4–6 mice per time point. Graphs depict data as mean ± SD (one-way ANOVA Tukey's multiple comparisons test, *$p < 0.05$, **$p < 0.01$; ***$p < 0.001$; ****$p < 0.0001$).

(F) Time course FACS analysis of Nb-infected lungs. Expression of indicated markers represented as t-SNE maps for Il18r1^{+} ILCs. ICS after incubation with PMA, ionomycin, and monensin. Data are pooled from 5 mice for each time point and merged from equal numbers of Lin^{-}Il7ra^{+} ILCs.

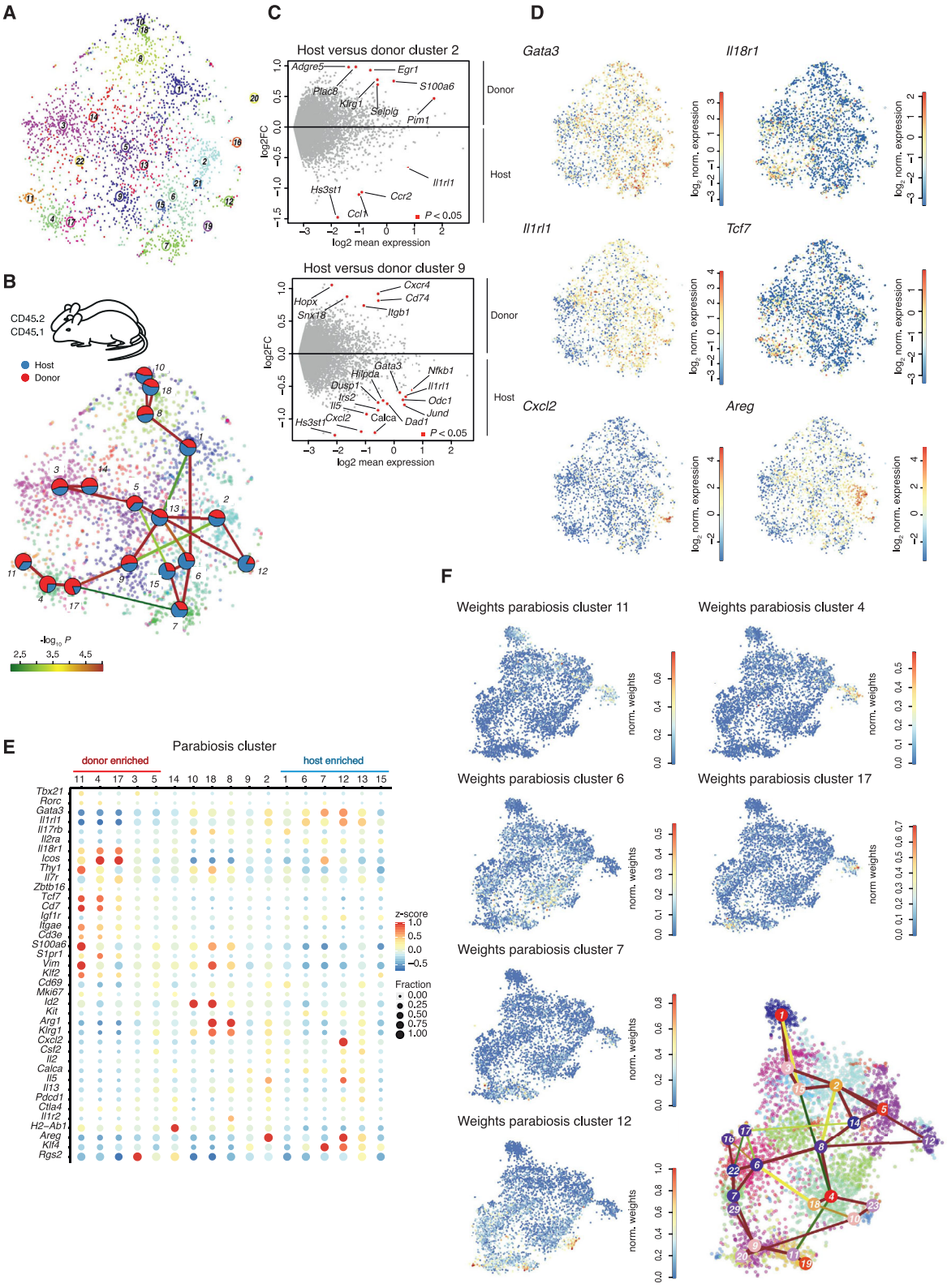

(legend on next page)

of less mature and migrating cells, consistent with their potential recruitment into the lung during infection. Our analyses did, however, not directly test this recruitment during infection, and donor-derived ILC2s could also differentiate from BM-derived cells that have migrated to tissues before infection. Consistent with both of these possibilities, our data established that the adult bone marrow is a source of ILC2s, which can traffic to the lung and can generate the full spectrum of ILC2 subsets and differentiation stages in the lung during infection.

DISCUSSION

Here, we examined how ILCs are maintained and regenerated in the adult organism and provide evidence that differentiation and maturation of ILC2s from immature progenitors occurs within the adult lung. We analyzed the full spectrum of lung ILC2s at single-cell resolution and identified a heterogeneous population of Il18r1$^+$ tissue-associated ILCs that express Tcf7 and Zbtb16 and low amounts of Gata3, ST2, and ILC2 effector molecules. We derived a continuous differentiation trajectory and validated the potential of Il18r1$^+$Tcf7$^+$ cells to differentiate into Gata3^{hi} ILC2s. Furthermore, single-cell transcriptome comparisons of ILC populations in the BM, neonatal, and adult lung at steady state, as well as over the course of helminth infection in wild-type, parabiotic, and shield chimeric mice support the idea that core programs of ILC2 differentiation are recapitulated during ontogeny as well as inflammatory challenge.

Systemic ILC progenitors in men exhibit a transcriptional profile reminiscent of Il18r1$^+$ ILCPs in murine lung (Ghaedi et al., 2020; Lim et al., 2017). We confirmed that these cells are present in human lung tissue and can be further characterized by IL18R1 and TCF1 expression. Our findings suggest that Il18r1$^+$ lung ILCPs represent the murine counterpart of human tissue ILCPs and thereby open new avenues to investigate how the local differentiation of tissue ILCs may contribute to inflammatory diseases (Mazzurana et al., 2018).

Il18 is best known as a myeloid-derived cytokine that can activate lymphocytes, including ILC2s (Ricardo-Gonzalez et al., 2018). Il18 may, however, have additional functions and Il18r1 should not be considered an exclusive marker of effector cells, because it is also expressed by BM hematopoietic stem cells (HSCs), common lymphoid progenitors, BM, and circulating ILCPs, (Lim et al., 2017; Seillet et al., 2016; Silberstein et al., 2016; Xu et al., 2019). Local production of Il18 regulates the turnover of HSCs in their niche (Silberstein et al., 2016). Future studies should therefore investigate the niches of Il18r1$^+$ ILC progenitors, as well as the potential functions of Il18 in regulating progenitor-like ILCs during homeostasis versus inflammatory challenge.

Il18r1$^+$ ILCs were virtually absent from peripheral blood of uninfected mice, but enriched in the lung vasculature, which harbors many leukocytes that marginate from the blood stream, enrich at the endothelium, and extravasate upon local inflammation (Anderson et al., 2014; Barletta et al., 2012; Yipp et al., 2017). It is therefore conceivable that the vasculature may similarly serve as a local reservoir or niche for subsets of Il18r1$^+$ ILCs. A large fraction of Il18r1$^+$ ILCs was nevertheless ivCD45$^-$, confirming their presence in the lung parenchyma. In addition, analysis of parabiotic mice suggested that these cells are resident or exchange only very slowly in the lung tissue. Importantly, lung-resident and BM ILCPs share core similarities. However, BM ILCPs were negative for *Il5* and *Il5*-fatemap label, while corresponding populations in the lung had intermediate levels of both, consistent with the idea that these cells receive local signals driving their maturation within the tissue. The lung has been proposed as a reservoir of HSCs (Lefrançais et al., 2017) and may provide niches for the local differentiation of progenitors. Consistent with local differentiation, pulmonary Il18r1$^+$ cells were highly proliferative in uninfected tissue (in striking contrast to BM ILCPs or mature tissue ILCs) and gave rise to Il18r1$^+$ST2$^-$, Il18r1$^+$ST2$^+$, and Il18r1$^-$ST2$^+$ ILCs in recipient lungs upon transfer. Transplanted mature ST2$^+$ cells, however, did not generate Il18r1$^+$ST2$^-$ or Il18r1$^+$ST2$^+$ populations, suggesting that they are further downstream of a differentiation cascade, or that they cannot access the niche of immature ILCs in the lung.

Our data raise the possibility that tissue ILCPs may locally self-renew, but also indicate that they can receive input from circulating cells. First, we observed a small but significant donor contribution in the ivCD45$^+$Il18r1$^+$CD103$^-$ subset in parabiotic mice. Second, we found that Il18r1$^+$Tcf7$^+$ immature cells are generated from donor BM in shield chimeras. Third, donor-populations in infected parabiotic and shield chimeric mice were enriched with Il18r1$^+$Tcf7$^+$ immature cells. Therefore, tissue ILCPs may receive low-grade influx from systemic counterparts. Increased competitive fitness of these cells may favor their contribution during aging or when the local tissue niches are reorganized (e.g., upon regeneration of the ILC pool after infection). Such a model may explain why the frequency of donor-derived ILC2s is low early on, but gradually increases several months after parabiotic surgery or in the reconstitution phase p.i. (Gasteiger et al., 2015; Huang et al., 2018; Ricardo-Gonzalez et al., 2020; Schneider et al., 2019). Despite a burst of ivCD45$^+$ migrating inflammatory cells in the acute phase of helminth infection, these studies consistently showed that the majority of ILC2s were derived from tissue-resident cells around 2 weeks p.i. Here, we provide evidence for the *in situ* differentiation of ILCs from resident progenitors, highlighting a mechanism for the local, tissue-autonomous maintenance of ILCs in the adult organism.

Figure 6. Recruited Cells Contribute to the Entire Phenotypic Spectrum of Lung ILC2s during *Nippostrongylus brasiliensis* Infection

(A) t-SNE map of cells derived from parabiotic mice at d15 p.i. highlighting RaceID3 clusters.

(B) StemID2 lineage inference and normalized donor and host contribution to clusters depicted as pie charts. Link color indicates p value of StemID2 links ($p < 0.05$, STAR Methods).

(C) Differentially expressed genes ($p < 0.05$, STAR Methods) between donor and host cells within the depicted clusters.

(D) t-SNE maps indicating log2 normalized expression of candidate genes in the parabiosis data.

(E) Expression of representative candidate genes for ILC subsets in parabiosis clusters with at least 20 cells. Color represents *Z* score of the mean expression across clusters, and dot size represents fraction of cells expressing the gene in the cluster.

(F) t-SNE map of parabiosis data showing normalized weights of indicated parabiosis cluster medoids for cells within the Nb time course data (cf. Figure 4) as computed by cluster mapping (STAR Methods).

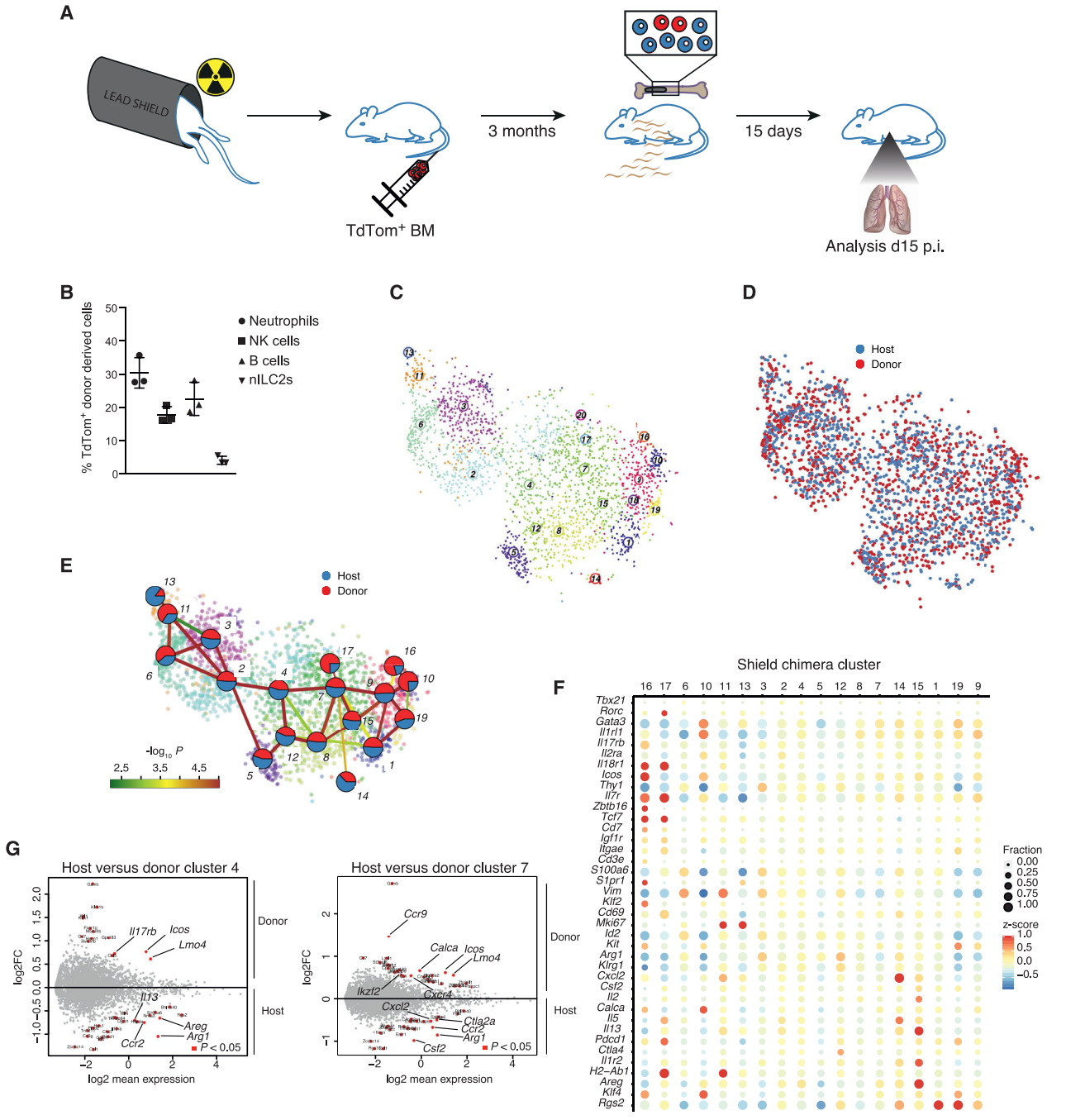

Figure 7. Bone Marrow-Derived ILCs Give Rise to the Full Phenotypic Spectrum of ILC2s in the Adult Lung

(A) Nb infection of the shield chimera model.

(B) Frequency of donor-derived cells from transferred bone marrow (BM).

(C and D) t-SNE map of ILCs from shield chimeric mice isolated at d15 p.i. highlighting RaceID3 clusters (C) and donor or host origin for each cell (D).

(E) StemID2 lineage inference and normalized donor and host contribution to clusters depicted as pie-charts. Link color indicates p value of StemID2 links ($p < 0.05$, STAR Methods).

(F) Expression of candidate genes for ILC subsets in the shield chimera clusters with at least 10 cells. Color represents *Z* score of the mean expression across clusters, and dot size represents fraction of cells expressing the gene in the cluster.

(G) Differentially expressed genes ($p < 0.05$, STAR Methods) between donor and host cells within the depicted clusters.

Importantly, we found that tissue ILCPs feature a phenotypic spectrum and mixed-lineage potential similar to the BM ILCP compartment. This heterogeneity may enable local "ILC-poiesis" to flexibly respond and generate the desired output upon distinct immune challenges.

Patients with inflammatory diseases such as psoriasis, hepatic fibrosis, or inflammatory bowel disease have elevated numbers of disease-associated ILCs in the blood. A major open question is how cells recruited during inflammation may contribute to the pool of tissue-resident cells. The extent to which local immune cells that have been generated early during ontogeny can be replenished in the adult organism has also been discussed for macrophages, representing prototypic tissue-resident cells (Ginhoux and Guilliams, 2016; Mass et al., 2016). Here, we found that adult BM cells recruited into the adult lung can generate the full spectrum of lung-resident ILC2 subsets upon helminth infection. Our analysis revealed that ILCs differentiating in the adult organism can locally adopt the phenotypes of ILCs that have been suggested to emerge in distinct waves during ontogeny (Popescu et al., 2019; Schneider et al., 2019). Therefore, local tissue niches, rather than progenitor origin, may dominantly imprint ILC phenotypes. Together, our work highlights the local differentiation of immature ILCs as a mechanism of maintenance, phenotypic diversification, and local adaptation of tissue ILCs.

Limitations of Study

One limitation in the study of ILCPs is the lack of conditional, stage-specific fate-mapping models to delineate the actual contribution of BM or tissue ILCPs during homeostasis or immune challenges in the adult organism. Moreover, we lack examples of conditions in which ILCPs are essential to maintain or regenerate a functional ILC pool. We speculate that ILCPs may have such critical roles upon depletion of ILCs, as documented in mice and men during different types of infection and environmental challenges (Kløverpris et al., 2016; Ng et al., 2018). It will be interesting to test whether local depletion and regeneration of ILC2s occurs during lung diseases as well. We are aware that our work highlights the tissue adaptation and differentiation potential of BM-derived ILCs in adult lungs but does not deconvolute potential contributions of other circulating cells. Future work should address if inflammatory ILC2s are a transient effector population or if (and how) they actually contribute to lung ILC2s once acute infection has resolved. Here, we mapped the heterogeneity of lung ILC2s and highlight multiple subsets that are dynamically emerging during infection, including, e.g., effector subsets expressing different combinations of cytokines and chemokines (Il5/Il2/Cxcl2/Csf2 versus Il5/Il13/Areg) or molecules involved in regulatory functions (Pd1, Ctla4, Il1r2, and MHCII) and highly proliferative Il18r1^{+} and/or CD103^{+} states. Although functional validation of these populations was beyond the scope of this study, our interactive cell atlas (http://murine-ilc-atlas.ie-freiburg.mpg.de/) provides a resource for future studies testing subset-specific functions of ILC2s.

STAR★METHODS

Detailed methods are provided in the online version of this paper and include the following:

- KEY RESOURCES TABLE
- RESOURCE AVAILABILITY
  - Lead Contact
  - Materials Availability
  - Accession Codes, Code and Data Availability
- EXPERIMENTAL MODEL AND SUBJECT DETAILS
  - Mice
- METHOD DETAILS
  - Parabiosis
  - Shield chimeras
  - ivCD45 labeling and murine cell isolation
  - Helminth Infection
  - Human samples and cell isolation
  - Antibody staining for sorting and flow cytometric analysis
  - Adoptive cell transfer
  - Cell culture of sorted ILCs subsets
  - Preparation of OP9/OP9-DL1 feeder cell layer
  - Single cell sorting, single-cell RNA amplification and library preparation of ILCs
  - Quantification of transcript abundance
  - Clustering
  - Cell-cycle Scoring
  - Lineage inference, pseudo-temporal ordering and SOM
  - KEGG/GO pathway enrichment
  - Fraction dot plot
  - Normalization of pie charts
  - Dataset integration
  - Cluster mapping: Inferring transcriptome similarities between two scRNA-seq datasets based on cluster annotation
- QUANTIFICATION AND STATISTICAL ANALYSIS
  - Differential expression analysis
  - Enrichment scores
- ADDITIONAL RESOURCES

SUPPLEMENTAL INFORMATION

Supplemental Information can be found online at https://doi.org/10.1016/j.immuni.2020.09.002.

ACKNOWLEDGMENTS

We thank A. Diefenbach, R. Golub, and W. Kastenmüller for critically reading the manuscript and G.A. Häcker and T. Gogishvilli for their support. This work was supported by grants through the German Research Foundation (DFG) priority program SPP1937-Innate lymphoid cells (GA2129/2-1 to G.G., GR4980/1-1 to D.G., RO3565/4-1 to C.R., and VO944/8-2 to D.V.) and the European Research Council (647257-STROMA to M.B., 759176-TissueLympho-Contexts to G.G., and 818846-ImmuNiche to D.G.). G.G. was further supported by the DFG Emmy Noether programme (GA2129/1-1). D.G. was further supported by the DFG (GR4980/3-1 and GRK2344 MeInBio), the DFG under Germany's Excellence Strategy (CIBSS-EXC-2189-Project 390939984), and by the Behrens-Weise-Foundation. G.G. and D.G. are supported by the Max Planck Society.

AUTHOR CONTRIBUTIONS

Conceptualization, funding acquisition, and project coordination, D.G. and G.G. scRNA-seq experiments, computational analysis, and web interface, P.Z. FACS analysis and transfers, M.L. *In vitro* culture experiments, M.L., P.Z., and J.S.H.; parabiosis, X.F. and S.E.; shield chimera, R.G.; human ILCs, D.C.H. Experimental support, K.K., N.P., C.F., R.D.-L., and A.M.K. Il5

reporter mouse, R.M.L. Nb culture, C.S. Experimental design, M.L., P.Z., D.G., and G.G. Supervision, A.R., D.V., M.B., C.R., D.G., and G.G. Paper writing and visualizations, P.Z., M.L., D.G., and G.G. Review and editing, all authors.

DECLARATION OF INTERESTS

The authors declare no competing interests.

Received: November 12, 2019
Revised: June 4, 2020
Accepted: September 8, 2020
Published: September 30, 2020

REFERENCES

Anders, S., and Huber, W. (2010). Differential expression analysis for sequence count data. Genome Biol. *11*, R106.

Anderson, K.G., Mayer-Barber, K., Sung, H., Beura, L., James, B.R., Taylor, J.J., Qunaj, L., Griffith, T.S., Vezys, V., Barber, D.L., and Masopust, D. (2014). Intravascular staining for discrimination of vascular and tissue leukocytes. Nat. Protoc. *9*, 209–222.

Baker, S.C., Bauer, S.R., Beyer, R.P., Brenton, J.D., Bromley, B., Burrill, J., Causton, H., Conley, M.P., Elespuru, R., Fero, M., et al.; External RNA Controls Consortium (2005). The external RNA controls consortium: A progress report. Nat. Methods *2*, 731–734.

Bando, J.K., Liang, H.-E., and Locksley, R.M. (2015). Identification and distribution of developing innate lymphoid cells in the fetal mouse intestine. Nat. Immunol. *16*, 153–160.

Baratin, M., Simon, L., Jorquera, A., Ghigo, C., Dembele, D., Nowak, J., Gentek, R., Wienert, S., Klauschen, F., Malissen, B., et al. (2017). T Cell Zone Resident Macrophages Silently Dispose of Apoptotic Cells in the Lymph Node. Immunity *47*, 349–362.

Barletta, K.E., Cagnina, R.E., Wallace, K.L., Ramos, S.I., Mehrad, B., and Linden, J. (2012). Leukocyte compartments in the mouse lung: distinguishing between marginated, interstitial, and alveolar cells in response to injury. J. Immunol. Methods *375*, 100–110.

Bielecki, P., Riesenfeld, S.J., Kowalczyk, M.S., Regev, A., and Flavell, R.A. (2018). Skin inflammation driven by differentiation of quiescent tissue-resident ILCs into a spectrum of pathogenic effectors. bioRxiv. https://doi.org/10.1101/461228.

Björklund, Å.K., Forkel, M., Picelli, S., Konya, V., Theorell, J., Friberg, D., Sandberg, R., and Mjösberg, J. (2016). The heterogeneity of human CD127 + innate lymphoid cells revealed by single-cell RNA sequencing. Nat. Immunol. *17*, 451–456.

Buettner, F., Natarajan, K.N., Casale, F.P., Proserpio, V., Scialdone, A., Theis, F.J., Teichmann, S.A., Marioni, J.C., and Stegle, O. (2015). Computational analysis of cell-to-cell heterogeneity in single-cell RNA-sequencing data reveals hidden subpopulations of cells. Nat. Biotechnol. *33*, 155–160.

Califano, D., Cho, J.J., Uddin, M.N., Lorentsen, K.J., Yang, Q., Bhandoola, A., Li, H., and Avram, D. (2015). Transcription Factor Bcl11b Controls Identity and Function of Mature Type 2 Innate Lymphoid Cells. Immunity *43*, 354–368.

Constantinides, M.G., McDonald, B.D., Verhoef, P.A., and Bendelac, A. (2014). A committed precursor to innate lymphoid cells. Nature *508*, 397–401.

Cuff, A.O., Robertson, F.P., Stegmann, K.A., Pallett, L.J., Maini, M.K., Davidson, B.R., and Male, V. (2016). Eomeshi NK Cells in Human Liver Are Long-Lived and Do Not Recirculate but Can Be Replenished from the Circulation. J. Immunol. *197*, 4283–4291.

Gasteiger, G., Fan, X., Dikiy, S., Lee, S.Y., and Rudensky, A.Y. (2015). Tissue residency of innate lymphoid cells in lymphoid and nonlymphoid organs. Science *350*, 981–985.

Gentek, R., Ghigo, C., Hoeffel, G., Bulle, M.J., Msallam, R., Gautier, G., Launay, P., Chen, J., Ginhoux, F., and Bajénoff, M. (2018). Hemogenic Endothelial Fate Mapping Reveals Dual Developmental Origin of Mast Cells. Immunity *48*, 1160–1171.

Ghaedi, M., Shen, Z.Y., Orangi, M., Martinez-Gonzalez, I., Wei, L., Lu, X., Das, A., Heravi-Moussavi, A., Marra, M.A., Bhandoola, A., and Takei, F. (2020). Single-cell analysis of RORα tracer mouse lung reveals ILC progenitors and effector ILC2 subsets. J. Exp. Med. *217*, jem.20182293.

Ghigo, C., Mondor, I., Jorquera, A., Nowak, J., Wienert, S., Zahner, S.P., Clausen, B.E., Luche, H., Malissen, B., Klauschen, F., and Bajénoff, M. (2013). Multicolor fate mapping of Langerhans cell homeostasis. J. Exp. Med. *210*, 1657–1664.

Ginhoux, F., and Guilliams, M. (2016). Tissue-Resident Macrophage Ontogeny and Homeostasis. Immunity *44*, 439–449.

Grün, D., Kester, L., and van Oudenaarden, A. (2014). Validation of noise models for single-cell transcriptomics. Nat. Methods *11*, 637–640.

Grün, D., Muraro, M.J., Boisset, J.-C., Wiebrands, K., Lyubimova, A., Dharmadhikari, G., van den Born, M., van Es, J., Jansen, E., Clevers, H., et al. (2016). De Novo Prediction of Stem Cell Identity using Single-Cell Transcriptome Data. Cell Stem Cell *19*, 266–277.

Hafemeister, C., and Satija, R. (2019). Normalization and variance stabilization of single-cell RNA-seq data using regularized negative binomial regression. Genome Biol. *20*, 296.

Harly, C., Kenney, D., Ren, G., Lai, B., Raabe, T., Yang, Q., Cam, M.C., Xue, H.-H., Zhao, K., and Bhandoola, A. (2019). The transcription factor TCF-1 enforces commitment to the innate lymphoid cell lineage. Nat. Immunol. *20*, 1150–1160.

Hashimshony, T., Senderovich, N., Avital, G., Klochendler, A., de Leeuw, Y., Anavy, L., Gennert, D., Li, S., Livak, K.J., Rozenblatt-Rosen, O., et al. (2016). CEL-Seq2: sensitive highly-multiplexed single-cell RNA-Seq. Genome Biol. *17*, 77.

Herman, J.S., Sagar, and Grün, D. (2018). FateID infers cell fate bias in multipotent progenitors from single-cell RNA-seq data. Nat. Methods *15*, 379–386.

Huang, Y., Mao, K., Chen, X., Sun, M.-A., Kawabe, T., Li, W., Usher, N., Zhu, J., Urban, J.F., Jr., Paul, W.E., and Germain, R.N. (2018). S1P-dependent interorgan trafficking of group 2 innate lymphoid cells supports host defense. Science *119*, 114–119.

Ishizuka, I.E., Chea, S., Gudjonson, H., Constantinides, M.G., Dinner, A.R., Bendelac, A., and Golub, R. (2016). Single-cell analysis defines the divergence between the innate lymphoid cell lineage and lymphoid tissue-inducer cell lineage. Nat. Immunol. *17*, 269–276.

Klose, C.S.N., Flach, M., Möhle, L., Rogell, L., Hoyler, T., Ebert, K., Fabiunke, C., Pfeifer, D., Sexl, V., Fonseca-Pereira, D., et al. (2014). Differentiation of type 1 ILCs from a common progenitor to all helper-like innate lymphoid cell lineages. Cell *157*, 340–356.

Kløverpris, H.N., Kazer, S.W., Mjösberg, J., Mabuka, J.M., Wellmann, A., Ndhlovu, Z., Yadon, M.C., Nhamoyebonde, S., Muenchhoff, M., Simoni, Y., et al. (2016). Innate Lymphoid Cells Are Depleted Irreversibly during Acute HIV-1 Infection in the Absence of Viral Suppression. Immunity *44*, 391–405.

Kobayashi, T., Voisin, B., Kim, D.Y., Kennedy, E.A., Jo, J.H., Shih, H.Y., Truong, A., Doebel, T., Sakamoto, K., Cui, C.Y., et al. (2019). Homeostatic Control of Sebaceous Glands by Innate Lymphoid Cells Regulates Commensal Bacteria Equilibrium. Cell *176*, 982–997.

Lefrançais, E., Ortiz-Muñoz, G., Caudrillier, A., Mallavia, B., Liu, F., Sayah, D.M., Thornton, E.E., Headley, M.B., David, T., Coughlin, S.R., et al. (2017). The lung is a site of platelet biogenesis and a reservoir for haematopoietic progenitors. Nature *544*, 105–109.

Li, H., and Durbin, R. (2010). Fast and accurate long-read alignment with Burrows-Wheeler transform. Bioinformatics *26*, 589–595.

Lim, A.I., Li, Y., Lopez-Lastra, S., Stadhouders, R., Paul, F., Casrouge, A., Serafini, N., Puel, A., Bustamante, J., Surace, L., et al. (2017). Systemic Human ILC Precursors Provide a Substrate for Tissue ILC Differentiation. Cell *168*, 1086–1100.

Lun, A., and Risso, D. (2019). SingleCellExperiment: S4 Classes for Single Cell Data. R package version v1.8.0.

Mass, E., Ballesteros, I., Farlik, M., Halbritter, F., Günther, P., Crozet, L., Jacome-Galarza, C.E., Händler, K., Klughammer, J., Kobayashi, Y., et al. (2016). Specification of tissue-resident macrophages during organogenesis. Science *353*, aaf4238.

Mazzurana, L., Rao, A., Van Acker, A., and Mjösberg, J. (2018). The roles for innate lymphoid cells in the human immune system. Semin. Immunopathol. *40*, 407–419.

Moro, K., Kabata, H., Tanabe, M., Koga, S., Takeno, N., Mochizuki, M., Fukunaga, K., Asano, K., Betsuyaku, T., and Koyasu, S. (2016). Interferon and IL-27 antagonize the function of group 2 innate lymphoid cells and type 2 innate immune responses. Nat. Immunol. *17*, 76–86.

Motran, C.C., Silvane, L., Chiapello, L.S., Theumer, M.G., Ambrosio, L.F., Volpini, X., Celias, D.P., and Cervi, L. (2018). Helminth Infections: Recognition and Modulation of the Immune Response by Innate Immune Cells. Front. Immunol. *9*, 664.

Nagasawa, M., Heesters, B.A., Kradolfer, C.M.A., Krabbendam, L., Martinez-Gonzalez, I., de Bruijn, M.J.W., Golebski, K., Hendriks, R.W., Stadhouders, R., Spits, H., and Bal, S.M. (2019). KLRG1 and NKp46 discriminate subpopulations of human CD117^{+}CRTH2^{-} ILCs biased toward ILC2 or ILC3. J. Exp. Med. *216*, 1762–1776.

Nagashima, H., Mahlakõiv, T., Shih, H.-Y., Davis, F.P., Meylan, F., Huang, Y., Harrison, O.J., Yao, C., Mikami, Y., Urban, J.F., Jr., et al. (2019). Neuropeptide CGRP Limits Group 2 Innate Lymphoid Cell Responses and Constrains Type 2 Inflammation. Immunity *51*, 682–695.

Nechanitzky, R., Akbas, D., Scherer, S., Hoyler, T., Ramamoorthy, S., Diefenbach, A., and Grosschedl, R. (2013). Transcription factor EBF1 is essential for the maintenance of B cell identity and prevention of alternative fates in committed cells. Nat. Immunology *14*, 867–875.

Ng, S.S., Souza-Fonseca-Guimaraes, F., Rivera, F.L., Amante, F.H., Kumar, R., Gao, Y., Sheel, M., Beattie, L., Montes de Oca, M., Guillerey, C., et al. (2018). Rapid loss of group 1 innate lymphoid cells during blood stage *Plasmodium* infection. Clin. Transl. Immunology *7*, e1003.

Nussbaum, J.C., Van Dyken, S.J., von Moltke, J., Cheng, L.E., Mohapatra, A., Molofsky, A.B., Thornton, E.E., Krummel, M.F., Chawla, A., Liang, H.-E., and Locksley, R.M. (2013). Type 2 innate lymphoid cells control eosinophil homeostasis. Nature *502*, 245–248.

Oherle, K., Acker, E., Bonfield, M., Wang, T., Gray, J., Lang, I., Bridges, J., Lewkowich, I., Xu, Y., Ahlfeld, S., et al. (2020). Insulin-like Growth Factor 1 Supports a Pulmonary Niche that Promotes Type 3 Innate Lymphoid Cell Development in Newborn Lungs. Immunity *52*, 275–294.

Oliphant, C.J., Hwang, Y.Y., Walker, J.A., Salimi, M., Wong, S.H., Brewer, J.M., Englezakis, A., Barlow, J.L., Hams, E., Scanlon, S.T., et al. (2014). MHCII-mediated dialog between group 2 innate lymphoid cells and CD4(+) T cells potentiates type 2 immunity and promotes parasitic helminth expulsion. Immunity *41*, 283–295.

Peng, H., Jiang, X., Chen, Y., Sojka, D.K., Wei, H., Gao, X., Sun, R., Yokoyama, W.M., and Tian, Z. (2013). Liver-resident NK cells confer adaptive immunity in skin-contact inflammation. J. Clin. Invest. *123*, 1444–1456.

Popescu, D.-M., Botting, R.A., Stephenson, E., Green, K., Webb, S., Jardine, L., Calderbank, E.F., Polanski, K., Goh, I., Efremova, M., et al. (2019). Decoding human fetal liver haematopoiesis. Nature *574*, 365–371.

Ricardo-Gonzalez, R.R., Van Dyken, S.J., Schneider, C., Lee, J., Nussbaum, J.C., Liang, H.E., Vaka, D., Eckalbar, W.L., Molofsky, A.B., Erle, D.J., and Locksley, R.M. (2018). Tissue signals imprint ILC2 identity with anticipatory function. Nat. Immunol. *19*, 1093–1099.

Ricardo-Gonzalez, R.R., Schneider, C., Liao, C., Lee, J., Liang, H.E., and Locksley, R.M. (2020). Tissue-specific pathways extrude activated ILC2s to disseminate type 2 immunity. J. Exp. Med. *217*, e20191172.

Robinette, M.L., Fuchs, A., Cortez, V.S., Lee, J.S., Wang, Y., Durum, S.K., Gilfillan, S., and Colonna, M.; Immunological Genome Consortium (2015). Transcriptional programs define molecular characteristics of innate lymphoid cell classes and subsets. Nat. Immunol. *16*, 306–317.

Sagar, Herman, J.S., Pospisilik, J.A., and Grün, D. (2018). High-Throughput Single-Cell RNA Sequencing and Data Analysis. Methods Mol. Biol. *1766*, 257–283.

Saluzzo, S., Gorki, A.-D., Rana, B.M.J., Martins, R., Scanlon, S., Starkl, P., Lakovits, K., Hladik, A., Korosec, A., Sharif, O., et al. (2017). First-Breath-Induced Type 2 Pathways Shape the Lung Immune Environment. Cell Rep. *18*, 1893–1905.

Schneider, C., Lee, J., Koga, S., Ricardo-Gonzalez, R.R., Nussbaum, J.C., Smith, L.K., Villeda, S.A., Liang, H.-E., and Locksley, R.M. (2019). Tissue-Resident Group 2 Innate Lymphoid Cells Differentiate by Layered Ontogeny and In Situ Perinatal Priming. Immunity *50*, 1425–1438.

Scott, C.L., Zheng, F., De Baetselier, P., Martens, L., Saeys, Y., De Prijck, S., Lippens, S., Abels, C., Schoonooghe, S., Raes, G., et al. (2016). Bone marrow-derived monocytes give rise to self-renewing and fully differentiated Kupffer cells. Nat. Commun. *7*, 10321.

Seehus, C.R., Aliahmad, P., de la Torre, B., Iliev, I.D., Spurka, L., Funari, V.A., and Kaye, J. (2015). The development of innate lymphoid cells requires TOX-dependent generation of a common innate lymphoid cell progenitor. Nat. Immunol. *16*, 599–608.

Seillet, C., Mielke, L.A., Amann-Zalcenstein, D.B., Su, S., Gao, J., Almeida, F.F., Shi, W., Ritchie, M.E., Naik, S.H., Huntington, N.D., et al. (2016). Deciphering the Innate Lymphoid Cell Transcriptional Program. Cell Rep. *17*, 436–447.

Silberstein, L., Goncalves, K.A., Kharchenko, P.V., Turcotte, R., Kfoury, Y., Mercier, F., Baryawno, N., Severe, N., Bachand, J., Spencer, J.A., et al. (2016). Proximity-Based Differential Single-Cell Analysis of the Niche to Identify Stem/Progenitor Cell Regulators. Cell Stem Cell *19*, 530–543.

Stier, M.T., Zhang, J., Goleniewska, K., Cephus, J.Y., Rusznak, M., Wu, L., Van Kaer, L., Zhou, B., Newcomb, D.C., and Peebles, R.S., Jr. (2018). IL-33 promotes the egress of group 2 innate lymphoid cells from the bone marrow. J. Exp. Med. *215*, 263–281.

Stuart, T., Butler, A., Hoffman, P., Hafemeister, C., Papalexi, E., Mauck, W.M., 3rd, Hao, Y., Stoeckius, M., Smibert, P., and Satija, R. (2019). Comprehensive Integration of Single-Cell Data. Cell *177*, 1888–1902.

Symowski, C., and Voehringer, D. (2019). Th2 cell-derived IL-4/IL-13 promote ILC2 accumulation in the lung by ILC2-intrinsic STAT6 signaling in mice. Eur. J. Immunol. *49*, 1421–1432.

Tirosh, I., Izar, B., Prakadan, S.M., Wadsworth, M.H., Treacy, D., Trombetta, J.J., Rotem, A., Rodman, C., Lian, C., Murphy, G., et al. (2016). Dissecting the multicellular ecosystem of metastatic melanoma by single-cell RNA-seq. Science *352*, 189–196.

Walker, J.A., Clark, P.A., Crisp, A., Barlow, J.L., Szeto, A., Ferreira, A.C.F., Rana, B.M.J., Jolin, H.E., Rodriguez-Rodriguez, N., Sivasubramaniam, M., et al. (2019). Polychromic Reporter Mice Reveal Unappreciated Innate Lymphoid Cell Progenitor Heterogeneity and Elusive ILC3 Progenitors in Bone Marrow. Immunity *51*, 104–118.

Wallrapp, A., Riesenfeld, S.J., Burkett, P.R., Abdulnour, R.E., Nyman, J., Dionne, D., Hofree, M., Cuoco, M.S., Rodman, C., Farouq, D., et al. (2017). The neuropeptide NMU amplifies ILC2-driven allergic lung inflammation. Nature *549*, 351–356.

Weiner, J., Zuber, J., Shonts, B., Yang, S., Fu, J., Martinez, M., Farber, D.L., Kato, T., and Sykes, M. (2017). Long-term Persistence of Innate Lymphoid Cells in the Gut After Intestinal Transplantation. Transplantation *101*, 2449–2454.

Wright, D.E., Wagers, A.J., Pathak Gulati, A., Johnson, F.L., and Weissman, I.L. (2001). Physiological migration of hematopoietic stem and progenitor cells. Science *294*, 1933–1936.

Xu, W., Cherrier, D.E., Chea, S., Vosshenrich, C., Serafini, N., Petit, M., Liu, P., Golub, R., and Di Santo, J.P. (2019). An Id2^{RFP}-Reporter Mouse Redefines Innate Lymphoid Cell Precursor Potentials. Immunity *50*, 1054–1068.

Yipp, B.G., Kim, J.H., Lima, R., Zbytnuik, L.D., Petri, B., Swanlund, N., Ho, M., Szeto, V.G., Tak, T., Koenderman, L., et al. (2017). The lung is a host defense niche for immediate neutrophil-mediated vascular protection. Sci. Immunol. *2*, eaam8929.

Yu, G., Wang, L.G., Han, Y., and He, Q.Y. (2012). clusterProfiler: an R package for comparing biological themes among gene clusters. OMICS *16*, 284–287.

Yu, Y., Wang, C., Clare, S., Wang, J., Lee, S.C., Brandt, C., Burke, S., Lu, L., He, D., Jenkins, N.A., et al. (2015). The transcription factor Bcl11b is specifically expressed in group 2 innate lymphoid cells and is essential for their development. J. Exp. Med. *212*, 865–874.